Evaluation of Emission Quantification Technologies

Interim Report

August 2nd, 2022

Prepared for:

Petroleum Technology Alliance Canada

and Clean Resources Innovation Network

Prepared by:

Professor Kyle J. Daun, PhD., P. Eng., FASME
Professor Christiane Lemieux, PhD
Professor Audrey Béliveau, PhD
Daniel Blackmore
Michael Nagorski
Kyu Min Shim
Paule Lapeyre
Augustine Wigle

University of Waterloo

Jack Johnson and Kevin Fritz

Arolytics, Inc.

Kirk Osadetz

CMC Research Institutes

EXECUTIVE SUMMARY

This report presents interim results from "Evaluation of Emission Quantification Technologies", a research program undertaken by the University of Waterloo (UW), Arolytics, Inc., and Carbon Management Canada (CMC) on behalf of the Petroleum Technology Alliance Canada (PTAC) and the Clean Resources Innovation Network (CRIN). The overall objective of this research is to survey candidate methane emissions quantification technologies and assess their performance under a range of industrially relevant scenarios. A key focus is placed on the estimation of uncertainty, which is endemic to emissions quantification.

Research tasks are divided into four phases: Phase 1 is a survey of candidate emission quantification technologies available to industry and their overall capability and suitability for various emissions scenarios; Phase 2 assesses the performance of candidate technologies through simulations and laboratory-scale measurements; Phase 3 is the planning and execution of field campaigns; and Phase 4 focuses on data analysis and detailed uncertainty quantification.

This report focuses on Phases 3 and 4, specifically the design, execution, and preliminary analysis of results from the first field campaign, held at CMC's Field Research Station in Newall County, Alberta, April 20-24, 2022. Five emission services providers or technology developers participated in the first field campaign, using four different quantification modalities: handheld quantitative optical gas imaging (QOGI), truck mounted tunable-diode laser-absorption spectroscopy (TDLAS), drone-mounted TDLAS, and airborne short-wavelength infrared (SWIR) hyperspectral imaging. Release rates were blind to the Providers, who were responsible for deriving their own emissions estimates from their measurements. In the case of the truck mounted TDLAS, a second analysis was carried out on the data by UW personnel using an alternative measurement model. Preliminary data analysis reveals that the quantification accuracy and precision of each technology is distinct and depends on emission rate and environmental factors in a unique way from the others.

The report concludes with a discussion of next steps, including planning for the second field campaign, planned for Fall 2022, and detailed uncertainty quantification (phase 4), which will be complete in 2023.

1. INTRODUCTION

As part of Canada's strategy to address climate change, the oil and gas sector is obligated to reduce methane emissions by 40-45% below 2012 levels by 2025. To meet these goals, and to fulfill their obligations under emerging provincial emission regulations, Canada's oil and gas producers need tools that can quantify methane emissions, in order to identify opportunities to reduce their overall emissions. Regulators also need methane quantification tools to assess compliance of industry to these regulations. Climate modellers need the data from these tools to understand how emissions from Canada's oil and gas industry contribute to climate change, which provincial governments and the Federal government will use to inform policy needed to fulfil Canada's international treaty obligations and to avoid the worst outcomes of climate change.

A diverse suite of candidate methane emission quantification tools is available to Canada's oil and gas industry. There is unlikely to be a "one-size-fits-all" solution: techniques designed to measure localized, persistent fugitive leaks from valves or gaskets may not be suitable for diffuse and intermittent emissions vented from storage tanks, surface casing vents, and CHOPS wells. Persistent emissions are identified reliably using periodic surveys, while highly variable or intermittent emissions may require continuous monitoring. Recent advancements in optoelectronic hardware (e.g., mid-wavelength infrared cameras, tunable diode laser spectroscopy, hyperspectral imaging) have augmented and disrupted the field of traditional concentration-based approaches, although their accuracy, precision, and best practices under various measurement scenarios are still being refined.

Choosing the "right tool for the job" depends, to a large extent, on the uncertainty associated with the methane emission estimates. This is particularly the case in a regulatory context. For example: How certain is it that an operator is complying with emissions? Is it reasonable to impose a limit on emissions that cannot be measured with reasonable accuracy? What is the most cost-effective technology to deploy for a given measurement scenario? To make these decisions, operators and regulators need to understand the uncertainty with which emissions may be quantified. Climate modellers and policy makers also need to understand the uncertainties attached to reported emission inventories in order to draft effective regulations that safeguard the environment without unduly penalizing oil and gas producers.

With these goals in mind, the Petroleum Technology Alliance Canada (PTAC) and Clean Resources Innovation Network (CRIN) engaged the University of Waterloo (UW), Arolytics, Inc. (Arolytics), and Carbon Management Canada, Inc. (CMC) to undertake a three-year research program entitled "Evaluation of Emission Quantification Technologies". The program is funded by the Alberta Upstream Petroleum Research Fund (AUPRF) through PTAC, the Government of Canada's Strategic Innovation Fund through CRIN, and the Natural Sciences and Engineering Research Council (NSERC).

The UW/Arolytics/CMC team brings together the diverse and complementary range of expertise and skills needed to fulfill these objectives. The UW team is led by Professor Kyle Daun from the Department of Mechanical and Mechatronics Engineering, an expert in optical gas imaging, laser-based diagnostics, remote sensing, and uncertainty quantification. Daun is joined by Professors Christiane Lemieux and Audrey Béliveau from the Department of Statistics and Actuarial Science. Lemieux's research interests focus on Monte Carlo simulations, while Béliveau studies Bayesian statistics and uncertainty quantification. Arolytics personnel working on the project include Julie Doan-Prévost, Jack Johnson, and Kevin Fritz. These personnel are experts in methane emissions

quantification and fugitive emission management programs (FEMPs); Johnson and Fritz also have extensive experience in methane emissions field measurements. Finally, CMC's participation is managed by Kirk Osadetz, a geoscientist and expert in methane emissions from Canada's oil and gas industry. Osadetz is CMC's Programs Development Manager and also manages CMC's Field Research Station, where candidate quantification technologies will be evaluated under industry-relevant conditions.

Research activities are organized into four project phases:

Phase 1: Quantification tool review interim summary table

Phase 2: Recommendation of viable quantification tools

Phase 3: Field campaign and execution

Phase 4: Data analysis and summary

These research activities are guided with input and oversight from PTAC, CRIN, and members of the Industrial Steering Committee (ISC), a subcommittee of PTAC's Air Research Planning Committee (ARPC).

Research progress in each of these phases is summarized in the following sections.

2. RESEARCH PROGRESS

2.1 Phase 1: Quantification tool review interim summary table (complete)

The initial project phase took place between September 2021 and February 2022 and was carried out by Doan-Prévost (Arolytics) and Daniel Blackmore, then an undergraduate research assistant working in Daun's lab at UW, with expert advice from Osadetz (CMC). The project commenced with a survey of available methane emission quantification technologies and an assessment of their cost, detection thresholds, and quantification accuracy. The research team also developed taxonomy charts that highlighted the operating principles of the technologies and their applicability to various measurement scenarios, and compiled a thorough literature review of independent performance studies. In total, 23 technologies were evaluated, and a subset of these were selected for more detailed analysis in Phases 2-4. These include truck-mounted tunable-diode laser-absorption spectroscopy (TDLAS); quantitative optical gas imaging (QOGI); and aircraft-based optical technologies.

The outcomes of this project phase were summarized in an earlier quarterly report. The summary table and diagrams are in Appendix A of this report.

2.2 Phase 2: Analysis of candidate emissions quantification technologies

This project phase has two components: Phase 2a, led by Arolytics; and Phase 2b, led by UW.

2.2.1: Phase 2a: Recommendation of the most viable quantification tools

Arolytics personnel will use Arolytics's proprietary AroFEMP simulation code to predict the performance of the technologies identified in Phase 1, were they incorporated into a fugitive emissions management program (FEMP). This procedure considers various simulation scenarios in which operators would use candidate technologies to detect and quantify methane emissions and then action repairs over a calendar year. Emission scenarios are sampled randomly from probability distributions that represent operational conditions, and emissions are detected and quantified with probabilities derived from manufacturer-specified characteristics of the quantification technologies or previous field trials identified in Phase 1. Many simulations are carried out via a Monte Carlo (MC) procedure and integrated to provide an expected reduction in emissions (e.g., m^3/year.)

In preparation for this project phase, Augustine Wigle, a UW PhD student under the supervision of Lemieux, spent a four-month internship with Arolytics to help them verify their code and improve its performance. (Wigle was sponsored by a Mitacs Accelerate Internship and paid outside of the project budget.) The next step in Phase 2a is to derive probabilities for representative emissions probability profiles. This will be done using data from the Fugitive Emission Management Program Effectiveness Assessment Study (FEMP-EA), a collection of fully randomized QOGI-based bottom-up emission measurements from approximately 200 oil and gas producing sites in the Red Deer region [1]. This data has only become available as of July 2022, so the AroFEMP simulation will be carried out later this year.

2.2.2: Phase 2b: Laboratory trials and development of digital twin systems

In parallel, the UW team is conducting laboratory-scale analysis and numerical simulations to further investigate the capabilities of the most promising technologies identified in Phase 1. Specifically, Phase 2b activities have focused on developing and quantifying the performance of spectroscopic and optical flow models for QOGI, and the derivation of an inverse Gaussian plume model (IGM) for interpreting truck based TDLAS measurements.

Research into QOGI technology is led by Michael Nagorski, an MASc candidate under Daun. Measurements were carried out using a FLIR GF320 camera and QL320 tablet system loaned from Professor Matthew Johnson at Carleton University, as well as a four-channel Telops multispectral (MS) channel provided by CMC. Nagorski developed an "in-house" version of the QL320 tablet based in Matlab® and validated its performance through simulated measurements generated using a CFD Large Eddy Simulation of a methane plume, as well as plumes generated with a heated vent apparatus in Daun's laboratory (Figure 1). The simulated measurements were used to validate the spectroscopic model used to infer the species column densities, and the optical flow algorithm used to obtain the velocity field [2, 3].

In the heated vent experiments, infrared images captured using the GF320 camera were interpreted using the QL320 tablet and UW's in-house code. In most cases, UW's code matched or exceeded the performance of the QL320 tablet with regards to the overall mass flow rate when using a bulk velocity estimated from the images, but the framerate of the GF320 was too low for the optical flow algorithm to provide robust velocity fields. These experiments highlighted measurement conditions that would be problematic for conducting QOGI emission estimates, especially emissive "white" plumes of uncertain temperatures. Since the GF320 camera has a single measurement spectrum, simultaneously inferring the methane column density (ppm·m) and temperature amounts to solving one equation with two unknowns. Consequently, it is necessary to assume a plume temperature when calculating emission rates in these scenarios; in cases where the plume temperature is uncertain, the corresponding emission rates may be highly inaccurate.

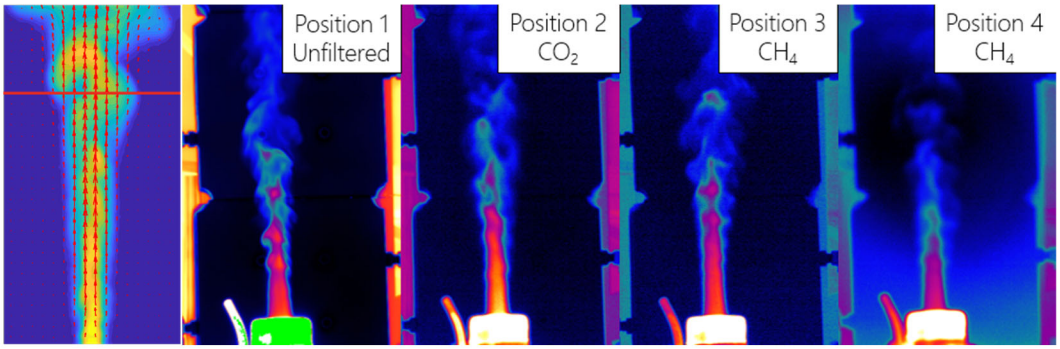

Figure 1: (left) Velocimetry on simulated data generated using a CFD-large eddy simulation. (right) Multispectral QOGI on the heated vent apparatus at UW.

The superior framerate of the Telops MS camera compared to the GF320 camera provided reliable velocimetry estimates. In principle it should be possible to infer plume temperature and column density simultaneously by comparing measurements made over different spectral windows, since the spectral distribution of emitted radiation varies with temperature in a predictable way (i.e., Planck's distribution). Unfortunately, while the single methane filter for the GF320 camera is cryogenically cooled, in the case of the Telops camera the filter wheel is uncooled, and blackbody emission from the warm filters contaminate the infrared images to an extent that cannot be removed through calibration. Multispectral cameras with actively cooled filters are under development and poised to dramatically improve the capabilities of QOGI [4].

Inverse Gaussian plume modelling (IGM) research is led by Blackmore, now an MASc student, with assistance from Dr. Paule Lapeyre, a postdoctoral fellow, both under Daun's supervision. The

IGM (Figure 2 [5]) was validated using concentrations from a CFD-Large Eddy Simulation of a methane plume, following Caulton, et al. [6]; these simulations were also used to evaluate how various factors (e.g., plume height, measurement location, wind speed) affect quantification uncertainty using this technique.

Both the QOGI and IGM measurement models have been deployed to interpret field measurements carried out in Phase 3. The IGM is also the basis for initial Bayesian uncertainty quantification analysis carried out under Phase 4.

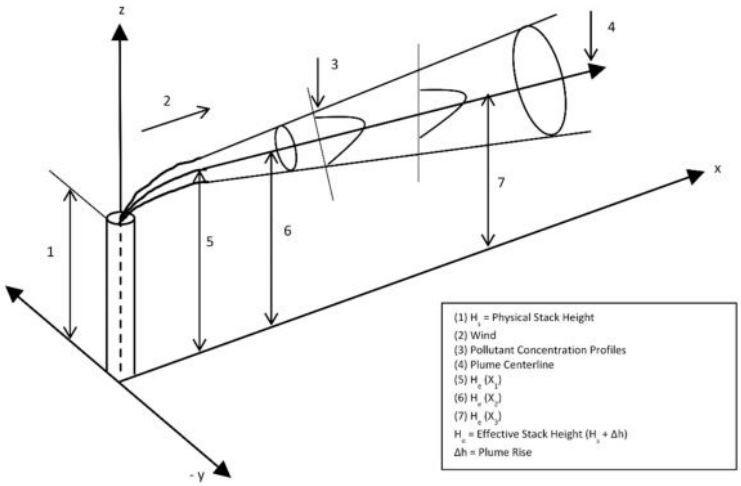

Figure 2: Schematic of an inverse Gaussian plume model (IGM) calculation [5].

2.3 Phase 3: Field campaign and execution

In the original research proposal, two field campaigns were planned: one in December 2021-January 2022, and a second one during the summer of 2022. The intention of scheduling two field campaigns at different times of the year was to highlight how different environmental factors (e.g., snow, air temperature, wind, moisture) may impact the availability and quantification accuracy of candidate technologies. However, due to the delayed start of the project, the first field campaign was postponed to April 20-26. The second field campaign is scheduled for September 25-October 1, with fallback dates of October 17-23. Environmental conditions during these times are expected to be similar, which will facilitate a comparison of the technologies between the field trials.

2.3.1 Location of the field campaigns

Field campaigns are held at CMC's Field Research Station (FRS), a 200 Ha site in Newall County, Alberta. The site, shown in Figure 3, is equipped with equipment that may be configured to mimic industrially relevant emission scenarios. These include tanks, surface casing and annulus vents, pneumatic actuators, and compressors, along with hoses, couplings, and emission stacks needed to generate the methane releases. A 13 m tall portable flare stack and a combustor were also located at the site, as part of a separate CanERIC-sponsored research program between CMC and the Southern Alberta Institute of Technology (SAIT).

The site is equipped with a Davis weather station (wind speed, wind direction, air temperature, and dew point) and two 3D ultrasonic anemometers: one attached to a rotating Kuva imaging system mounted to a gantry (~16 m above ground), and one belonging to the University of

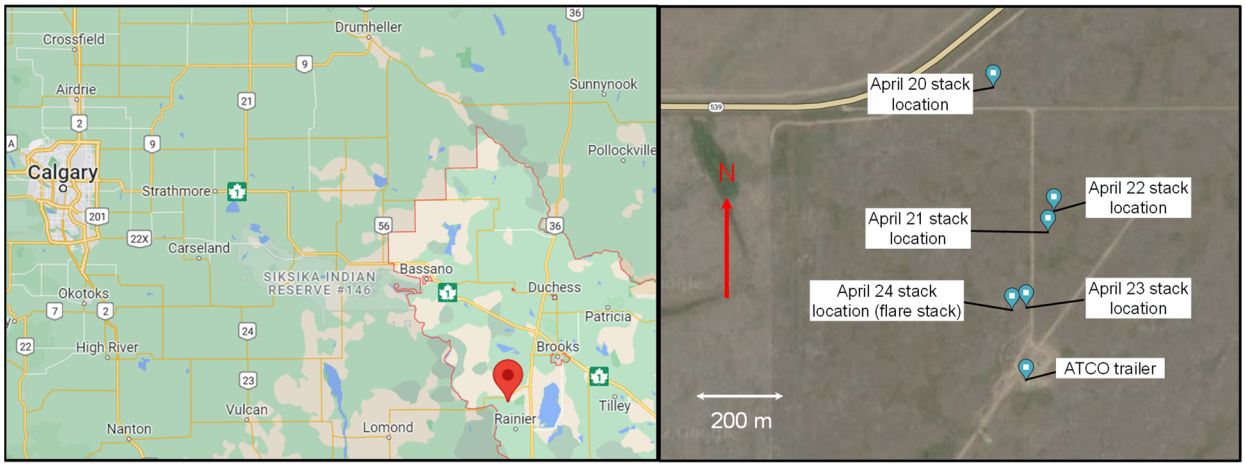

Figure 3: Location of CMC's Field Research Station in Newall County, AB.

Figure 4: Participants of the first field campaign included two QOGI systems, truck- and drone-mounted TDLAS, and airborne SWIR hyperspectral imaging.

Colorado (UC). The UC anemometer was inoperable during the first field campaign, but it will be used in the second field campaign.

2.3.2 Planning for the first field campaign

Planning for the first field trial began in January 2022, led by Arolytics (Johnson) with input from Daun (UW) and Osadetz (CMC). Based on the outcome of Phase 1, and after consultation with the ISC, 17 candidate service or technology providers were invited to participate in the field trials. These providers, summarized in Appendix B, were organized into three classes: the inspection class (QOGI, stationary sensors, and drone-based TDLAS); screening class (truck-based measurements); and the rapid screening class (aircraft). Of these providers, seven applied to participate in the field campaign, and ultimately the five providers listed in Table 1 agreed to participate in the campaign. Unfortunately, Telops/LSI had to cancel their participation due to a servicing issue with the aircraft.

Based on these participants and detection classes, and with input from the ISC, a testing matrix was developed that captured emission scenarios relevant to Canada's upstream oil and gas industry. Key considerations in the design of the field campaign were as follows:

1. Tank emissions, e.g., from thief hatches, represent a significant component of overall emission inventories, and are also very difficult to measure using QOGI due to the difficulty of accessing the release and the complex flow patterns in the wake of the tank. Accordingly, a subset of releases took place from the top of a storage tank.
2. Emission rates inferred using plume models and truck mounted TDLAS are sensitive to emission height. Moreover, wind speed, which varies with height above ground, is also known to play a significant role in quantification accuracy. Therefore, emissions were planned from a range of release heights.
3. Smaller emissions from individual components may be quantifiable using inspection- or screening-class technologies, but airborne-based sensors generally have higher detection thresholds. Accordingly, emission rates were different for the ground-based and airborne platforms.
4. The US EPA recently proposed a 10 kg/hr minimum detection threshold for candidate methane detection technologies under Section 111 of the Clean Air Act [7].
5. While the focus of this study is on quantification uncertainty of known emissions, detection is a key concern and is a significant factor in the uncertainty of overall emission inventories [8]. Therefore, several releases are "null releases" in which no methane was released. The technology providers were unaware of these null releases.

Technology providers were responsible for all ancillary information needed to construct emissions estimates from their measurements (e.g., wind speed, ambient temperature), and were not provided any additional information other than the emission location.

2.3.3 Execution of the first field campaign

Testing was scheduled for five days, April 20-24, with April 25 and 26 reserved for weather days. Due to favorable weather conditions, testing was completed on April 24. As noted in Table 1, the truck and AGAT QOGI were only available on the first three days, while the SAIT drone, GHGSat aircraft, and UW QOGI were available on the final two days.

Table 1: Technology providers for the first field campaign.

Class	**Technology**	**Provider**	**Dates**
Inspection	QOGI (FLIR GF320/QL320)	AGAT[1]	Sep 20, 21, 22
		SAIT/UW[1,2]	Sep 22, 23, 24
	Drone-mounted TDLAS	SAIT	Sep 23, 24
Screening	Truck-mounted TDLAS	Boreal	Sep 20, 21, 22
Rapid Screening	Airborne SWIR HS	GHGSat	Sep 23, 24
	Airborne LWIR HS	Telops/LSI	Did not attend

1. The SAIT and AGAT QOGI systems were both FLIR GF320/QL320, but different software versions of the tablet.
2. The SAIT QOGI system was operated by UW personnel (Nagorski)

Ambient conditions

Meteorological conditions may have a pronounced influence on the effectiveness of most quantification technologies. In the case of QOGI, for example, high winds both dilute a methane release and may confound the feature tracking used to infer plume velocity, while uncertain plume temperature can affect the performance of the spectroscopic submodel used by QOGI systems to determine column densities. Uncertainty in wind conditions is also a leading source of error for truck- and drone-mounted TDLAS measurements and airborne measurements, since, unlike QOGI, these techniques use wind speed as an input to the advective transport model that converts

concentrations or column densities to a mass flow rate. The situation is particularly acute for the airborne measurements, since they do not generally have access to ground-based anemometry and instead must rely on weather models [8, 9]. Accordingly, wind speed, wind direction, temperature, and dew point were recorded throughout the tests; this instrumentation is summarized in Table 2. Whenever possible these parameters were measured by multiple independent sensors and compared with predictions from the Meteoblue weather model to provide an indication of uncertainty. This information will be crucial to the uncertainty quantification accuracies that will be undertaken in Phase 4.

Weather conditions at the FRS during the field trials are summarized in Appendix D. In general, all instrumentation produced consistent results. For the remainder of the analysis, wind speed is taken to be from the Kuva 3D ultrasonic anemometer since it was available throughout the field campaign and is more sensitive than the Davis cup-and-ball anemometer. Wind speeds were typically between 0-10 m/s, with a median value of 4 m/s. Air temperature ranged from −5°C to 20°C. An analysis of 10 years of historical meteorological data at the FRS shows that conditions during the field campaign were typical of what one would expect at this location and this time of year.

Since the airborne SWIR imager used by the GHGSat team infers methane column densities from the attenuation of sunlight reflected from the ground, sky condition is expected to be a significant factor in the effectiveness of this technology. Sky coverage is taken from the Meteoblue model and compared with observations from nearby airports made every three hours.

Temporal variations in both regional and local background methane concentrations can also affect inferred emission rates, sometimes significantly. Both regional oil and gas operations and several feedlots and water wells, most of which are in the Lethbridge coal zone, could contribute to significant and temporally-varying background methane concentrations at the FRS. Accordingly, the local background methane concentration was monitored continuously during the tests using a Picarro cavity ring-down spectrometer (CRDS), rented from the FluxLab at St. Francis Xavier University. The CRDS was located in the ATCO trailer (Figure 3), and sampled air via a hose through a window. Additional local background concentrations are obtained from TDLAS measurements from the Boreal truck and the SAIT drone when these vehicles were outside of a methane plume release. Previous measurements of local background methane concentrations and their variations were available from 2019 and 2020 observations using a dual frequency comb laser spectrometer constructed by Longpath Technologies LLC, of Boulder Co. and the Université Laval, QC.

The observed local backgrounds during these tests were mostly consistent with dual comb laser attenuation measurements, which observed normal local methane backgrounds to vary between about 1.85 ppm and 2.10 ppm. Background methane concentrations remained near regional average atmospheric abundance (~2 ppm) except for April 23, when the concentration rose abruptly to 3-4 ppm, with a maximum reading of 7 ppm. An accompanying rise in background ethane concentration recorded by the CRDS suggests that the local background anomaly was likely associated with upstream petroleum operations [10]. However, intermittent emissions from upstream petroleum equipment and agricultural water wells in the immediate vicinity of the FRS were observed to produce background methane concentration anomalies of approximately 0 to 120 ppb in 2019 and 2020. Instead, given the wind direction on April 23, and methane composition used in our test it is likely that this detection was caused by our own tests.

Table 2: Instrumentation used to characterize ambient conditions

Instrument	Data	Availability	Notes
3D ultrasonic anemometer	Wind speed and direction	Throughout campaign	Attached to Kuva station, near ATCO trailer. Rotating, so wind direction is uncertain
3D ultrasonic anemometer	Wind speed and direction	April 20-22	Stationary, part of Boreal (truck) measurement system
Davis weather station (cup anemometer, hygrometer, RTD sensor)	Wind speed and direction, temperature, relative humidity	Throughout campaign	Mounted on ATCO trailer
Picarro cavity ring-down spectrometer	Background CH_4 CH_4/C_2H_6, isotopes	Throughout campaign	Located at ATCO trailer
TDLAS	Background methane concentration	April 20-22	Mobile, part of Boreal (truck) measurement system
TDLAS	Background methane concentration	April 23-24	Attached to SAIT drone

Release schedule and measurements

Methane was released from pressurized gas cylinders located in a trailer, through a heat exchanger (Figure 5), and subsequently through a mass flow controller (Alicat Model MCR-2000SLPM-D-PAR, calibrated March 29, 2021). The methane temperature dropped significantly as it was released from the pressurized cylinders due to the Joule-Thomson effect and so the heat exchanger was used to return the methane to ambient air temperature. Periodic measurements of the methane discharge temperature at the nozzle exit carried out throughout the tests confirmed that the discharge temperature matched that of the surrounding air. The composition of the released gas was determined, as the average of five samples analyzed by gas chromatography, to be 94.2% methane, 3.4% ethane, 1.1% propane and 1.3% other minor components, predominantly N_2 and O_2 in roughly relative atmospheric abundances [11].

Four distinct measurement scenarios were considered: emissions from the top of a 2.79 m storage tank, a 1.42 m tall stack, a 3.18 m tall tack, and a 13 m tall unlit flare (Figure 6). Release rates ranged from 0.25 kg/hr (5.81 SLPM) to 50 kg/hr (1164 SLPM); this range was chosen based on industrially relevant emission scenarios and the manufacturer-specified capabilities of the instruments. The combination of emission scenarios and release rates corresponded with 47 distinct release events, summarized in Table 3, with several duplicated conditions. A subset of these emissions were null emissions. Most releases lasted approximately 10-50 minutes (longer releases for the airborne measurements), with an interval of at least 5 minutes between releases to ensure that any residual methane from the previous release had been conveyed from the area by the wind. The emission rates were chosen quasi-randomly, to disguise the emission rate from the provider and avoid artificial correlations between release rate and wind speed, since the latter quantity tends to increase or decrease monotonically with time.

Service or technology providers carried out measurements throughout the releases, although care was taken to ensure that the release rate was not adjusted during the measurements. Table 4 summarizes the number of detections/measurement events per provider. Figure 7 (a) shows a histogram of the ground truth release rates for the 383 measurement events, while Figure 7 (b) shows that these emission rates were generally uncorrelated with wind speed.

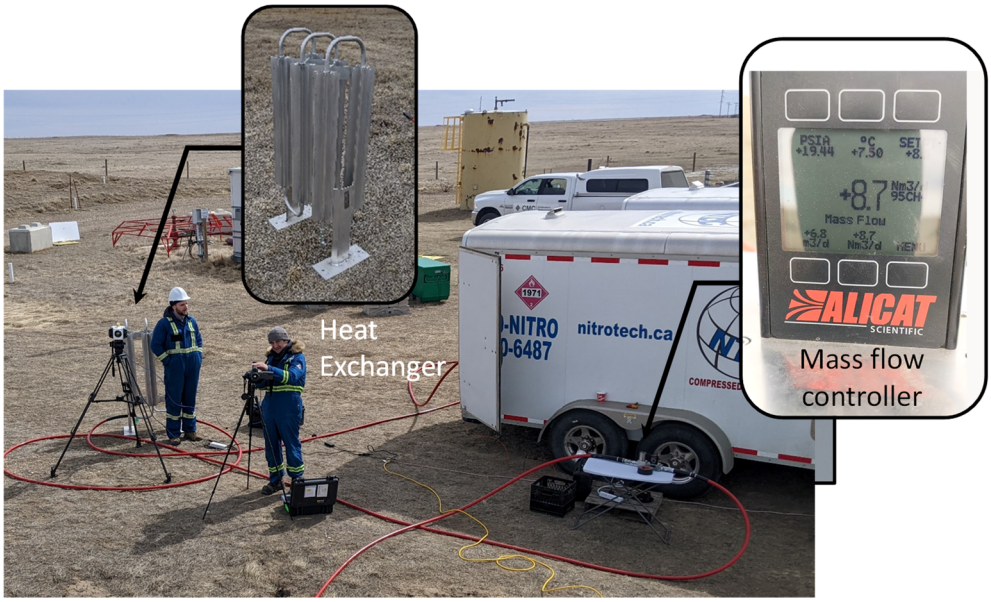

Figure 5: Methane was released from compressed cylinders in a trailer, through a heat exchanger, and then into a mass flow meter, before exiting a nozzle, stack, or the unlit flare.

Figure 6: Methane release scenarios included a 2.79 m tall storage tank, a 1.42 m tall stack, a 3.18 m tall stack, and a 13 m tall flare. The flare was unlit for methane emission measurements.

Table 3: Release scenarios for the first field campaign.

April 20	**April 21**	**April 22**	**April 23**	**April 24**
AGAT QOGI, Truck	AGAT QOGI, Truck	AGAT QOGI, Truck	Aircraft, Drone, UW QOGI[1]	Aircraft, Drone, UW QOGI
1.42 m stack (0, 1, 2.46, 5, and 10 kg/hr)	Storage tank (0, 1, 2.46, 5, and 10 kg/hr) 1.42 m stack (20 and 30 kg/hr)	1.42 m stack (0, 0.25, 0.5, 1, 2.46, 5 kg/hr)	3.18 m stack (20, 30, 40 50 kg/hr) 1.42 m stack (5 kg/hr) UW QOGI and drone	Unlit flare (0, 10, 20, 30, 40, 50, 80 kg/hr)

Table 4: Number of measurement events per technology for the first field campaign.

	April 20	**April 21**	**April 22**	**April 23**	**April 24**	**Total**
AGAT QOGI	36	48	37			121
UW QOGI				9	6	15
Truck	36 (2)	77	39 (2)			152 (4)
Drone			1*	8 (6)	6 (2)	15 (8)
Aircraft				44	36	80
Total	72 (2)	125	77 (2)	61	48	383 (4)

() denote missed detections, * denote missing measurement event

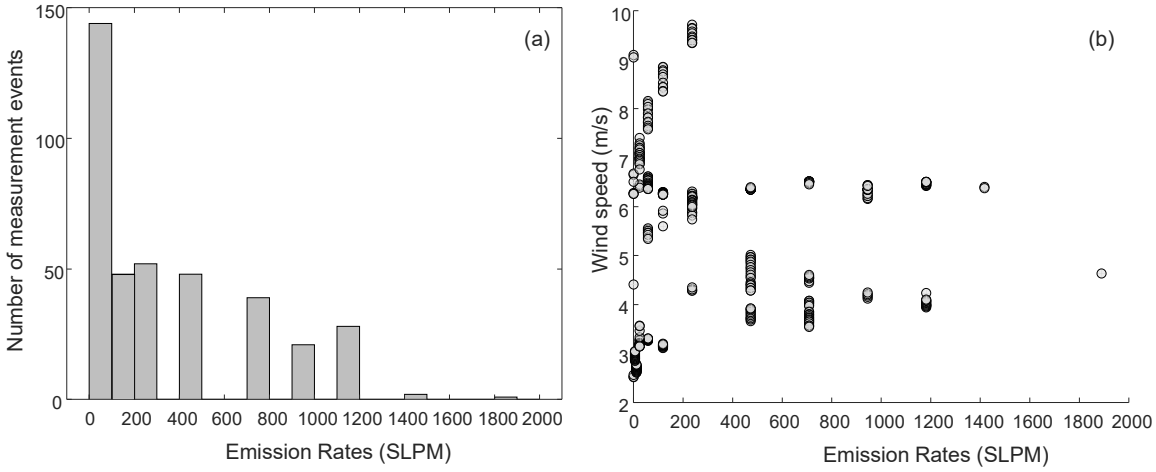

Figure 7: (a) Histogram of ground truth release rates for the measurement events; (b) plot of wind speed vs. ground truth release rate.

Providers were responsible for converting their field measurements (QOGI images, TDLAS concentrations, wind speeds, or SWIR hyperspectral images) into methane release rates. The research team asked the providers to provide their estimates within 2-3 weeks of the measurements, which, with one exception, was satisfied. Specific comments for each provider are provided below:

QOGI: QOGI measurements were carried out by AGAT personnel using a FLIR GF320 camera (24° fixed lens) and a Providence Photonics QL320 Tablet (Version 3.0.0.5). UW personnel conducted additional QOGI measurements using a FLIR GFx320 (24° fixed lens) and a FLIR QL320 tablet (Version 1.4.1). Both the camera and the tablet used by the UW team are newer than the ones used by AGAT. The AGAT surveyor also measured plume temperature using a Thomas Scientific hygrometer-thermometer-barometer probe, which was then input into the QL320 tablet to calculate the methane flow rate. Both teams carried out measurements in a manner consistent with FLIR QOGI training, i.e., using tripods, avoiding non-uniform clouds, measuring temperature and distance. Raw data consisted of mp4 files and radiometric video files that were post-processed with the QL320 tablet and the UW in-house algorithm. An example of the methane releases captured using the SAIT GFx320/QL320 system is shown in Figure 8.

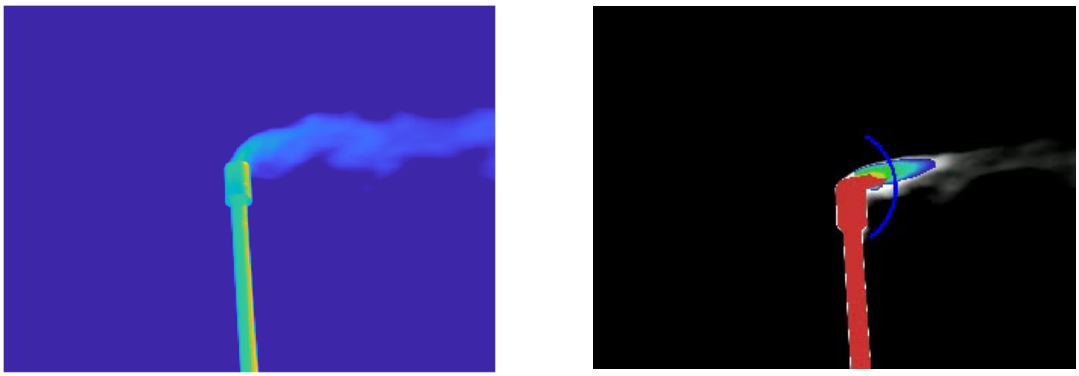

Figure 8: Methane plume as viewed using the GF320 camera (left) and the QL320 tablet (right). Note the curved control surface used for mass flux calculations.

Truck-mounted TDLAS: The truck carried out several plume transects at various distances from the release point; an example measurement path is shown in Figure 9 (a). The provider set up a GPS ground station and a 3D anemometer at the beginning of each testing day. Raw data consisted of TDLAS-derived concentrations, GPS tracks, and wind speed and direction recorded at intervals of every 15 minutes. Plume transects were conducted over three days, with concentration and GPS measurements taken every one second during the transect, and anemometry data being recorded at 15-minute intervals.

The provider analyzed the data using Wind-Trax, a backwards Lagrangian stochastic (BLS) dispersion model developed at the University of Alberta [12, 13]. The Wind-Trax model is based on a reduced transport equation:

$$\frac{\partial c}{\partial t} + \mathbf{u} \cdot \nabla c = 0 \tag{1}$$

where $c(\mathbf{x})$ is the point concentration of methane at a location $\mathbf{x} = [x, y, z]^{\mathrm{T}}$, and $\boldsymbol{u} = [u, v, w]^{\mathrm{T}}$ is the wind vector with components in the x-, y-, and z- direction [14]. The model assumes idealized wind conditions for undisturbed terrain, and requires inputs including the measured methane concentration, background concentration, and meteorological data such as the average wind speed and the measured sonic temperature [15]. The emission rate from a particular source location is estimated by determining the trajectories of particles, and projecting these trajectories backwards in time to an emission source to infer a leak rate. This method is described in detail in Ref. [16].

The provider also gave the raw data to the UW team, who conducted an independent analysis using the IGM approach [6]. The IGM is based on a Gaussian plume model, which assumes that the time-averaged concentration field from a steady release is given by

$$c(\mathbf{x}) = \frac{Q}{2\pi\mu\sigma_x\sigma_y}\left\{\exp\left[-\frac{(z-h)^2}{2\sigma_z^2}\right] + \exp\left[-\frac{(z+h)^2}{2\sigma_z^2}\right]\right\}\exp\left(-\frac{y^2}{2\sigma_z^2}\right) \tag{2}$$

where $\mathbf{x} = [x, y, z]^{\mathrm{T}}$ refers to a specific downwind (x) and crosswind (y) location, and height (z) relative to the source location, Q is the mass emission rate of the gas, μ is the wind speed at the release height, h is the effective release height, and σ_y and σ_z are coefficients relating to the atmospheric conditions. In the IGM procedure, Equation (2) is inverted to solve for Q using concentration measurements obtained by the technology. By using the raw data provided by Boreal

Laser, the performance of IGM and BLS was compared using the same concentration dataset and supporting anemometry data.

Drone-mounted TDLAS: The drone flew a descending helical flight pattern around each release, as shown in Figure 9 (b). The altitude and radius of this pattern were adjusted heuristically based on wind speed and emission height. Raw data consisted of concentration, drone altitude, and GPS coordinates. In principle, wind speed and wind direction can be inferred from the drone flight parameters and the plume direction. Emission rates were then inferred from mass balance conducted on a control surface defined by the helical flightpath of the drone. The drone team remarked that the number of drone transits through each plume, which was limited by the interval with which the release rate was adjusted, was considerably lower than what they would normally use when conducting independent measurements.

Airborne SWIR HS: Aircraft measurements were done at an altitude of approximately 1500 m (5,000 ft.). The provider had the GPS location of the release, and flew repeated passes around the release, as shown in Figure 9 (c). The provider was not aware of the release height. The flight path was roughly aligned with the wind direction, which was southerly during April 23 and April 24; this also coincides with the FRS access road, which is aligned to grid north. The provider used an internal algorithm (similar to the one described in Ref. [9]) to extract column densities from the SWIR measurements, based on the attenuation of reflected sunlight. This data is then combined with wind speeds obtained from Meteoblue to obtain the emission estimates.

A preliminary analysis of this data is presented in Section 3 of this report.

2.3.4 Planning for the second field campaign

The Arolytics/UW/CMC team started planning for the second field campaign shortly after the completion of the first field campaign. This activity is led by Arolyics (Fritz, Johnson), with assistance from Daun (UW) and Osadetz (CMC). The second campaign is currently scheduled for September 25-October 1, with fallback dates of October 17-23. The team is currently in discussion with several service or technology providers to participate, including three aircraft-conveyed technologies (GHGSat, LSI/Telops, Bridger) and a truck-based provider (Montrose). The team also intends to conduct additional QOGI measurements, either via a commercial provider or by having UW personnel operate a FLIR GF320/QL320 system.

The inclusion of the three aerially-conveyed technologies is particularly exciting since they all operate according to different spectroscopic principles and have anticipated strengths and weaknesses. As already described, GHGSat uses a short-wavelength infrared (SWIR) hyperspectral camera to image sunlight reflected from the ground to calculate the methane column density between the ground and the aircraft. LSI/Telops also uses a hyperspectral camera, but one that operates in the long-wavelength infrared (LWIR), and measures thermal radiation emitted by the methane plume. Both approaches are fully passive, in that the aircraft does not actively illuminate the plume, but otherwise they are quite different and have contrasting strengths and weaknesses: GHGSat is susceptible to overcast conditions and ground having low reflectance (e.g., covered in snow or water), while the Telops system relies on the emitted plume having a detectable temperature difference from that of the background (e.g., the terrain).

The third system, provided by Bridger, uses a scanning airborne TDLAS system. In contrast to the drone-based TDLAS, in which the optical path is contained within the instrument, the Bridger system scans the ground with the laser in an elliptical pattern, and infers the methane column

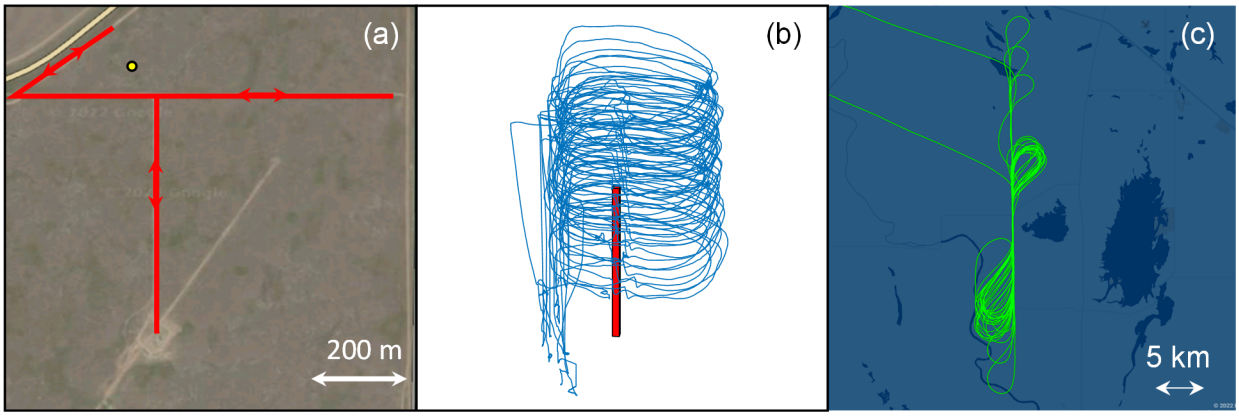

Figure 9: Typical measurement paths of the (a) truck, (b) drone, and (c) aircraft.

density from the reflected laser light. This active illumination system contrasts with the GHGSat and Telops systems, which are purely passive.

In all three cases, the optical data is interpreted with a spectroscopic model (similar to the one used for QOGI cameras) to produce a 2D column density map, or, in the case of the Bridger system, a 3D plume concentration map, by exploiting the change in angle as the aircraft overflies the plume. The column densities/concentrations are then combined with an advection model informed from local wind estimates to find the mass flow rates.

A key lesson learned from the first field campaign concerns wind speed and emission rate, two of the leading factors that affect quantification accuracy. As shown in Figure 7 (b), the strategy of assigning emission rates following a random pattern to avoid correlations with wind speed was largely successful, although there are "gaps" in the wind speed/emission rate map. These gaps will be filled during the second field campaign as allowed by the weather conditions by scheduling emission rates according to projected diurnal wind variations. Furthermore, analysis of the Meteoblue sky coverage model showed significant differences between predicted and observed cloud coverage. Sky condition will also be photographed at hourly intervals throughout the airborne measurements during the second field campaign.

2.4 Phase 4: Data analysis and summary

2.4.1: Overview of results

Emissions Service Provider-reported emission estimates are summarized in Figure 10, along with the ground-truth emission rates and wind speeds from the Kuva anemometer. The results show no obvious overall trend in emission quantification accuracy versus wind speed, nor emission quantification accuracy versus emission rate, although, as one may expect, larger emission rates correspond to larger emission residuals. Provider-reported emission rates, on average, underestimate the true emission rates. Estimates from the drone are excluded from this figure for reasons explained later in this report.

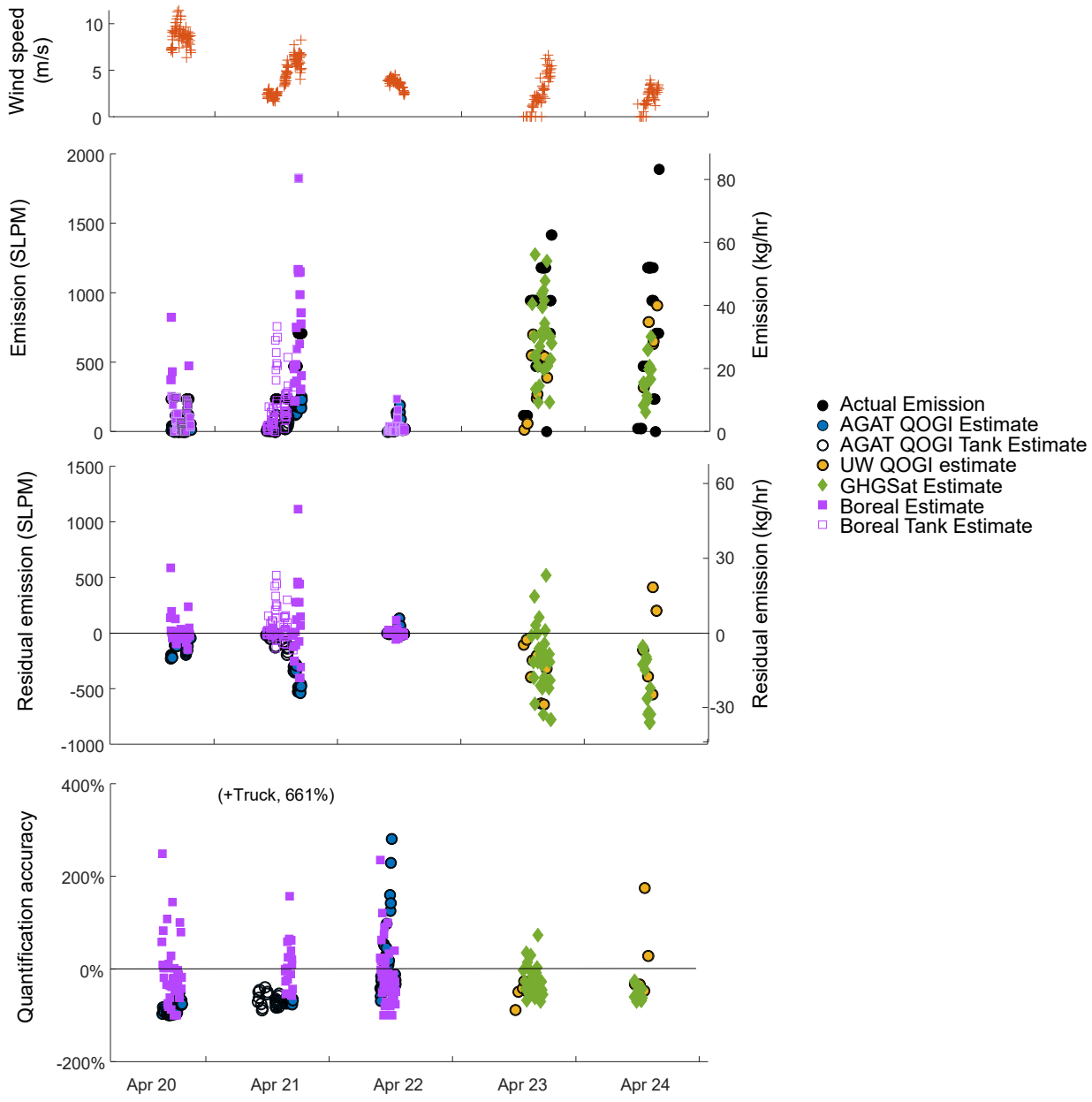

Figure 10: Summary of emission quantification accuracy and wind speed. (All technologies).

2.4.2 Quantitative Optical Gas Imaging

The accuracy of emission estimates obtained from the GF320/QL320 systems are shown in Figure 11. Estimates from the AGAT QOGI are summarized in Figures 12 (a) and (b) for emissions from the stack and from the top of the tank, respectively.

Overall, the performance of QOGI for measuring methane plumes emitted from the tank was slightly worse than the emissions from the stack. We suspect that this difference is largely due to the fact that the QOGI measurement of the tank release was carried out on the ground, as shown in Figure 5 (for safety reasons) and thus the measurement distance between the camera and the plume was much greater than in the case of the stack releases. It is well known that measurement distance is one of the major factors in QOGI quantification accuracy [17, 18]. The effect of measurement distance will be explored via a more rigorous test procedure in the second field campaign.

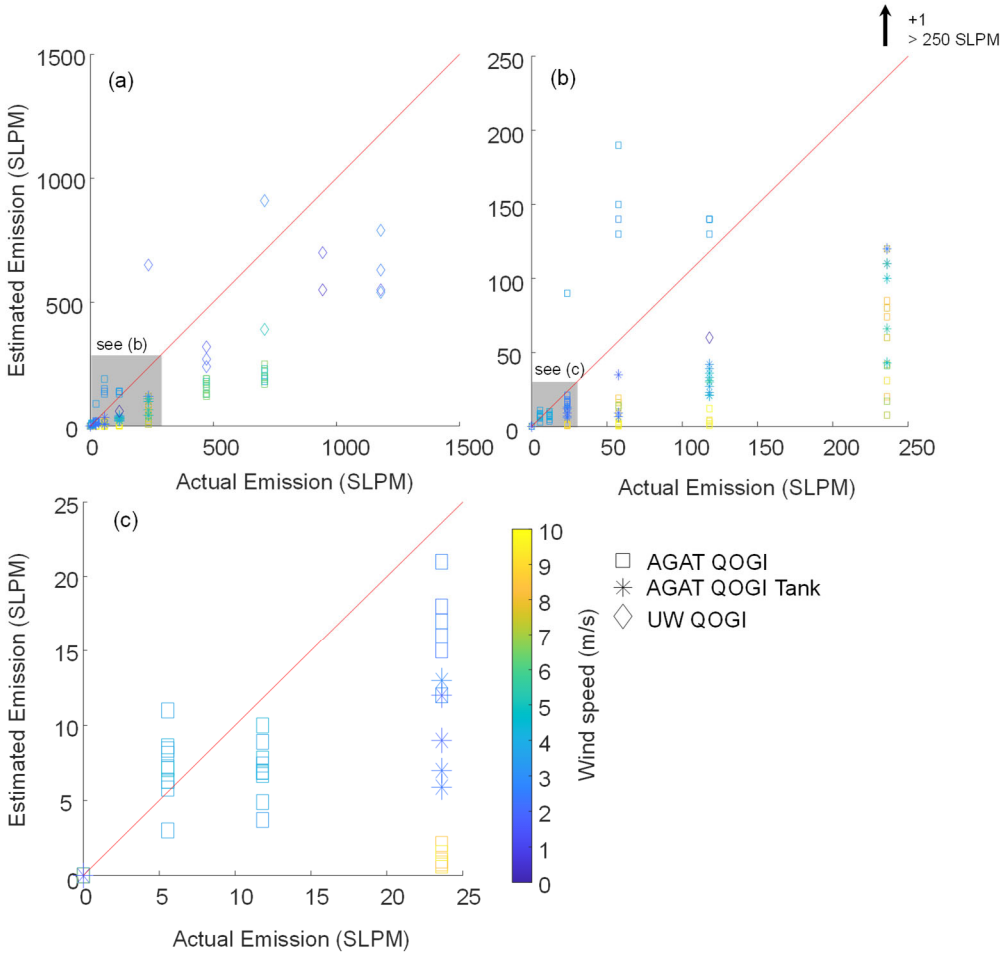

Figure 11: Performance of QOGI technologies. (a) All emission rates; (b) Emission rates less than 250 SLPM (11 kg/hr); (c) Emission rates less than 25 SLPM (1.1 kg/hr). Symbol color denotes wind speed. Hollow symbols denote stack measurements, while "*" indicates tank measurement.

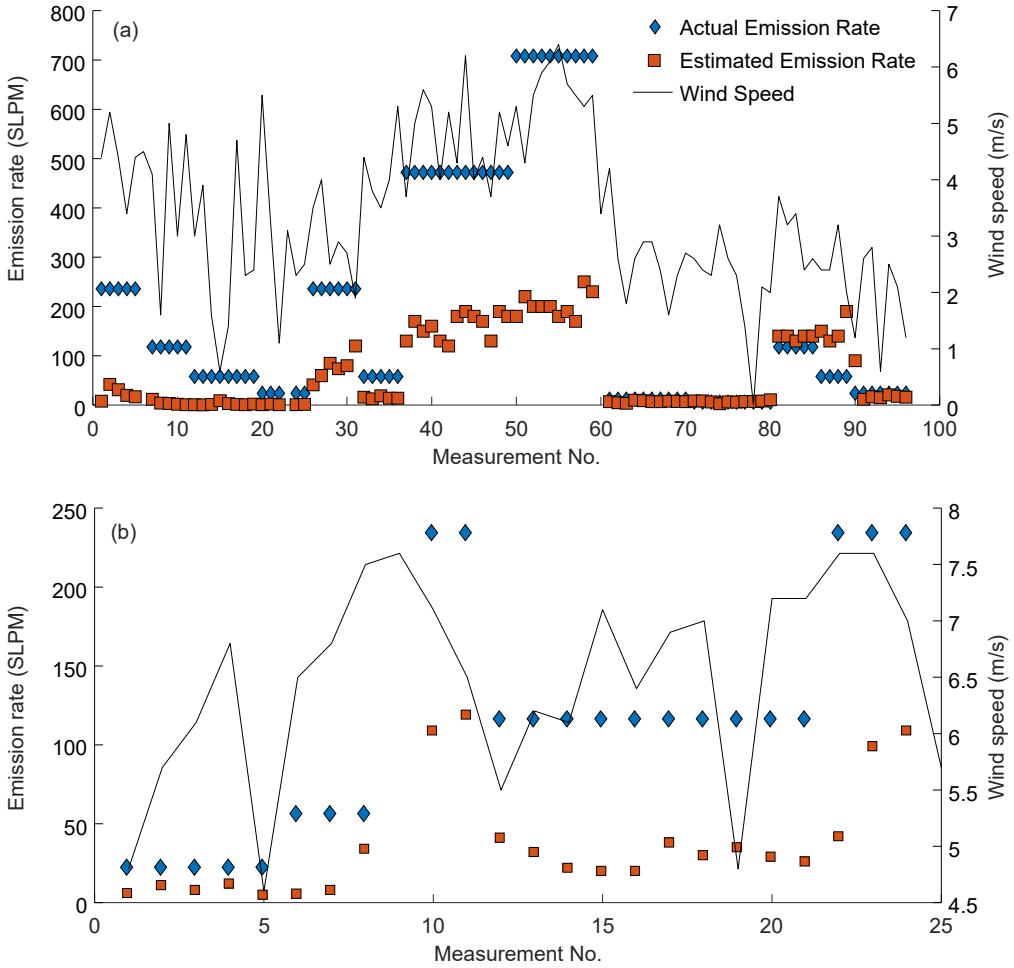

Figure 12: Quantification estimates from the AGAT-operated QOGI for (a) emissions from the stack and (b) emissions from the top of the tank.

AGAT QOGI: Measurements were carried out on April 20-22 on emissions from the 1.42 m stack and the storage tank. For emission rates of 236 SLPM (10 kg/hr) and greater, the QL320 consistently under-predicts the actual emission rate by 50% to 97%. It is unlikely that the camera has an upper detection limit in terms of the column densities produced by large emission rates; a more plausible explanation is that the QOGI hardware or software is unable to accurately estimate the velocities at these higher rates.

As seen in Figure 11 (b), at the 236 SLPM emission rate, increasing wind speed led to lower QOGI estimates and larger errors. This supports the hypothesis that the GF320/QL320 system has an upper limit for the velocities it can estimate accurately. Larger emission rates and higher wind speeds lead to faster gas velocities which require a higher camera frame rate to fully capture the plume motion. Higher wind speeds also result in greater plume dispersion and smaller column densities which may approach the sensitivity limit of the camera, but more in-depth analysis of the radiometric sequence files obtained and discussed in the following section showed this is not the primary source of error.

For emission rates below 236 SLPM (10 kg/hr), the QL320 still tends to under-predict the actual emission rate but at the lowest rate of 6 SLPM (0.25 kg/hr) the estimates almost entirely over-

predicted the actual rate. This testing regime includes a number of null releases, which were identified correctly by the AGAT QOGI operator.

UW QOGI: Measurements were made on methane releases from the 1.42 and 3.18 m tall stacks and the 13 m unlit flare; these results are summarized in Table 5. The GFx320/QL320 system only became available to UW on April 23, so no head-to-head comparison was possible between the UW and AGAT systems and operators.

The release rates from the 3.18 m tall stack were amongst the largest used in the current field trial. QL320 estimates from the UW operator were slightly more accurate (45% lower) than the estimates from AGAT (68% lower) for these large release rates. This result may appear counterintuitive since the AGAT QOGI operator is considerably more experienced than the UW operator, and a recent study highlighted that operator experience is a key factor in the accuracy of QOGI performance [18]. However, the AGAT QOGI tablet is a much earlier version compared to the SAIT tablet, and it appears that the manufacturer made significant improvements to the velocimetry algorithm between these versions.

Measurements of releases from an unlit flare (which have been shown to be an unexpectedly large contribution to overall methane emissions [19]) were also made and the QL320 estimates ranged from 47% lower to 175% higher than the actual release rate. Overestimates of measurements 14 and 15 are likely due to the very low wind speeds, which required the operator to wait for the plume to develop and cross the control surface (see Figure 8) while it meandered. This behaviour would lead to momentarily higher column density estimates compared to that expected for a steady plume of the same emission rate.

The UW team also analyzed raw radiometric files from the GF320 camera using their own spectroscopic model. The retrieved column densities were plausible and consistent with the ground-truth emission rates when they were combined with a bulk velocity inferred from the apparent plume motion between successive frames.

Table 5: QOGI measurements conducted by UW

Measurement	Estimated emission rate (SLPM)	Actual emission rate (SLPM)	Error (%)	Wind speed (m/s)	Distance (m)	Setup
1	14	118	-88%	-	3.23	1.42 m stack
2	60	118	-49%	6.6	3.83	1.42 m stack
3	550	944	-42%	6.6	4.88	3.18 m stack
4	700	944	-26%	6.0	4.01	3.18 m stack
5	240	472	-49%	5.7	4.01	3.18 m stack
6	270	472	-43%	6.6	3	3.18 m stack
7	550	1181	-53%	5.6	4.01	3.18 m stack
8	540	1181	-54%	4.5	3	3.18 m stack
9	390	708	-45%	5.1	3	3.18 m stack
10	0	24	N/A	4.0	11	Unlit flare
11	320	472	-32%	5.8	11	Unlit flare
12	790	1181	-33%	3.6	11	Unlit flare
13	630	1181	-47%	2.9	11	Unlit flare
14	650	236	175%	1.2	11	Unlit flare
15	910	708	28%	2.2	11	Unlit flare

2.4.3 Truck-mounted TDLAS

Truck-mounted TDLAS measurements were performed from April 20-22 on emissions from the 1.42 m stack and the top of the storage tank. Emission estimates obtained by the technology provider using the BLS measurement and wind speeds measured using a ground-based ultrasonic anemometer are summarized in Figure 13 and Table 6. Overall, the BLS method had an average absolute error of 57% for all emissions, with an average bias of +19%.

On the whole the estimates obtained from the truck mounted TDLAS/BLS measurements were the most accurate and least biased of all techniques. Estimates were less accurate for smaller release rates. It is also apparent that estimates of emissions released by the stack were much more accurate than those from the top of the tank. It can be seen through the highly positive average bias that the emission rates from the tank were systematically overestimated. The origin of these trends is currently under investigation.

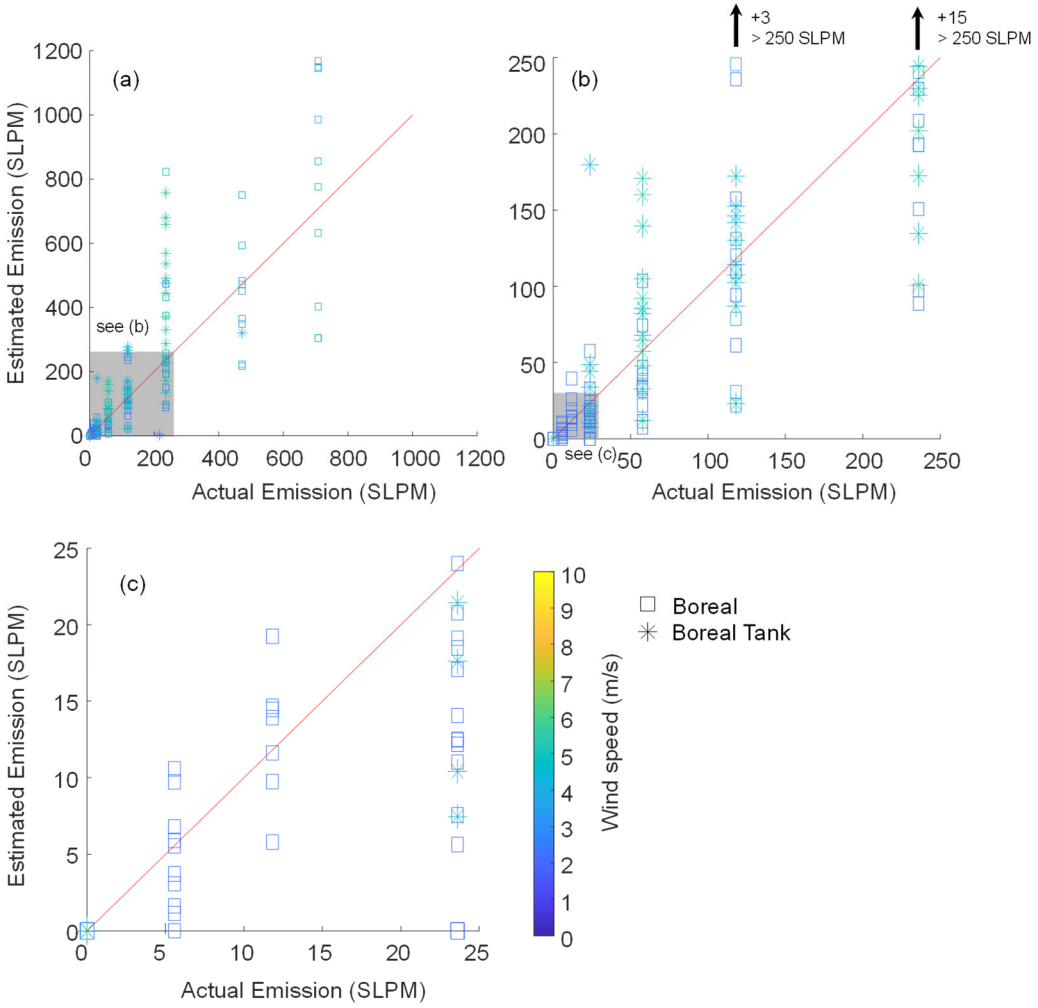

Figure 13: Performance of truck-mounted TDLAS using backwards Lagrangian stochastic (BLS) model. (a) All emission rates; (b) Emission rates less than 250 SLPM (11 kg/hr); (c) Emission rates less than 25 SLPM (1.1 kg/hr). Symbol color denotes wind speed. Hollow symbols denote stack measurements, while "*" indicates tank measurement

Table 6: Emissions obtained using truck mounted TDLAS

Release Type/Rate	BLS		IGM	
	Average Error[1]	Average Bias[2]	Average Error[1]	Average Bias[2]
Stack	47.06%	–5.87%	45.90%	–35.14%
Tank	72.06%	+44.56%	53.47%	–35.06%
<250 SLPM	59.51%	+15.28%	45.59%	–33.78%
<25 SLPM	62.27%	+2.99%	46.64%	–36.62%
>250 SLPM	41.09%	+6.82%	58.29%	–46.19%
ALL	56.89%	+18.77%	46.97%	–35.13%

[1]Defined as the average absolute relative error, ave(|ε|)
[2]Defined as the average relative error, ave(ε)

Preliminary emission estimates from the IGM are shown in Figure 14. The IGM analysis performed on the same dataset is comparable in accuracy with the BLS analysis (IGM: 50.21%, BLS: 56.89%). On the other hand, there was a stronger bias associated with the IGM analysis, with an average bias of -36.12% across all emission estimates. In total 87% of the IGM estimates underestimate the true emission rate, compared to 53% of the BLS estimates.

Ongoing work is focused on understanding why the IGM analysis consistently underestimates the emission rates. One explanation is the coarse meteorological data used in the analysis. Meteorological data from the Boreal anemometer was available in 15-minute increments, while concentration measurements used in the analysis were taken every second. During the measurements, the wind direction was observed to change during a plume transect, leading to inaccurate wind data for the IGM analysis. This is of particular importance to IGM, as the wind direction is key in determining the downwind distance from the source location to the measurement location. This downwind distance is used to calculate the dispersion parameters σ_y and σ_z in Equation (2), which sensitizes IGM-derived emissions to wind-direction. Conversely, the BLS analysis does not explicitly include the downwind distance, and instead relies on the backwards trajectories of particles to determine a source location, which may make BLS-derived emission rates less susceptible to errors in wind direction.

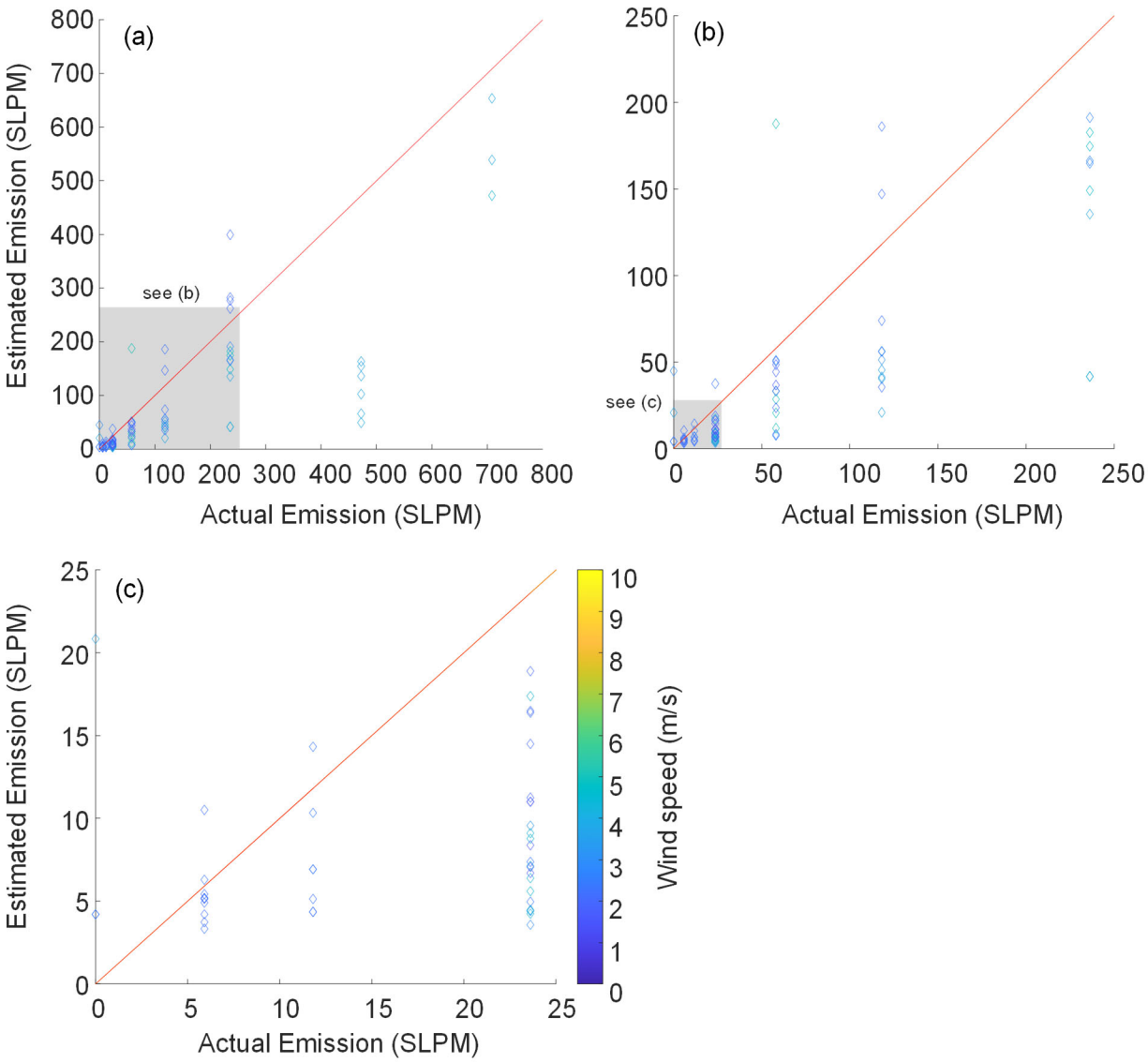

Figure 14: Performance of truck-mounted TDLAS using the inverse Gaussian plume model (IGM). (a) All emission rates; (b) Emission rates less than 250 SLPM (11 kg/hr); (c) Emission rates less than 25 SLPM (1.1 kg/hr). Symbol color denotes wind speed. Hollow symbols denote stack measurements, while "*" indicates tank measurement

2.4.4 Drone-mounted TDLAS

As noted in Section 2.3, the drone flies a descending helical path around the release, and the local methane concentration is measured with an onboard open-path TDLAS sensor. These concentrations are combined with GPS and barometric altimeter telemetry and wind speeds to obtain an emission rate estimate. Figure 15 shows an example of the data collected from the drone, while emission rates derived from the drone are plotted in Figure 16.

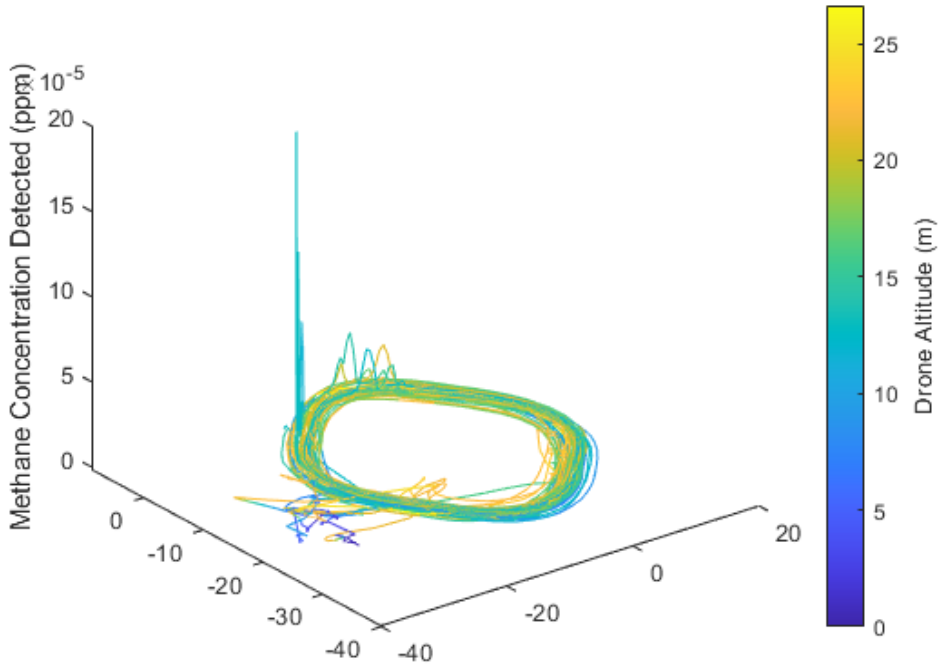

Figure 15: Example concentration and telemetry data obtained from a drone flight for a release from the unlit flare (13 m).

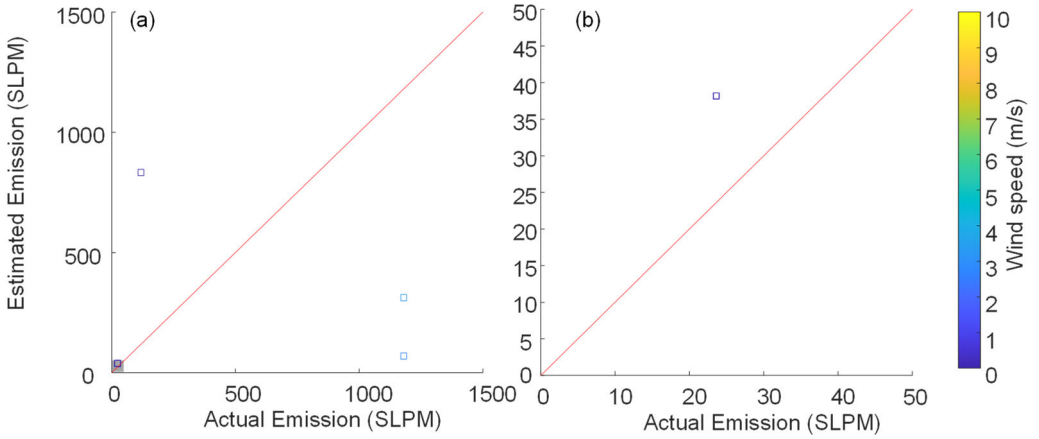

Figure 16: Performance of drone-mounted TDLAS. (a) All emission rates. (b) Emission rates below 50 SLPM (2.14 kg/hr).

In total 15 measurements were attempted by the SAIT team, but only 14 emission events were reported. (One emission event, on April 22, appears to have been missed in the analysis.) As shown in Table 7, of these measurements, the majority (8) were considered as missed detections. Reasons for missed detections included: "no data," which we interpret as a failure in telemetry between the drone and the data logger; "unstable wind," which we interpret as a plume that moved appreciably during the helical flight path shown in Figure 9 (b); and "too low plume to measure with drone", which referred to the fact that the emission leaving the stack was driven into the ground by the ambient air motion, so that most of the plume was missed by the drone.

To support the last observation, SAIT personnel conducted several smoke releases tests to visualize the methane plume. In these tests, a smoke canister was placed on the top of the 1.42 m stack and activated. While smoke particles are heavier than methane, the smoke is hot, so a smoke plume and a methane plume should have similar buoyancies. These tests, one of which is shown in Figure 17, revealed that the wind conditions appear to be pushing the smoke downwards, which supported the SAIT's contention that, in some cases, the plume was too close to the ground to be measured effectively by the drone.

Table 7: Summary of SAIT drone measurements.

Number of Measurements	Emission Reported	Technology Provider Comments
8	No	No data
1	Yes	No aerial data. Inverse Gaussian plume estimate – slightly unstable wind
1	Yes	Poor aerial data – most of plume too low to measure with the drone
1	Yes	Insufficient data
3	Yes	None

Figure 17: Example smoke release test. The dispersion of smoke suggested that the ambient wind was pushing the methane towards the ground.

2.4.4 Airborne SWIR HS

Airborne SWIR emission rates were carried out by GHGSat on April 23 (3.18 m stack) and April 24 (13 m unlit flare). On both days the Provider remarked that the weather conditions were suboptimal due to partial cloud cover. This was particularly the case on April 24, and measurements were terminated at approximately 2:30 PM due to excessive cloud cover. A detailed discussion of cloud cover is provided in Appendix D.

Figure 18 compares the GHGSat estimates with ground truth releases. The results show that the emissions estimated from the airborne SWIR imaging systematically under-predict the true emission rates. There are two reasons why this may be so: (1) methane column densities may be under-predicted due to cloud cover; (2) wind speeds used to derive the emission rate may be underestimated.

Cloud cover: Since methane column densities are inferred from the attenuation of sunlight reflected from the ground and imaged by the airborne SWIR imaging spectrometer, it is possible that cloud cover may cause a portion of the plume being missed. As detailed in Appendix D, the Meteoblue cloud cover model was found to be inaccurate during the measurements, and no systematic sky observations were made during the tests. This hypothesis could be explored by examining visible and SWIR images taken by the Provider during the measurement campaign, should they decide to provide this data.

Inaccurate wind speed: Our present understanding is that GHGSat obtains the wind speed from the Meteoblue model. These wind speeds are combined with column densities via a plume advection mode and transformed into an overall emissions estimate. It is therefore possible that the emission rates could be systematically underestimated because the wind assumed by the technology provider is lower than the true wind speed.

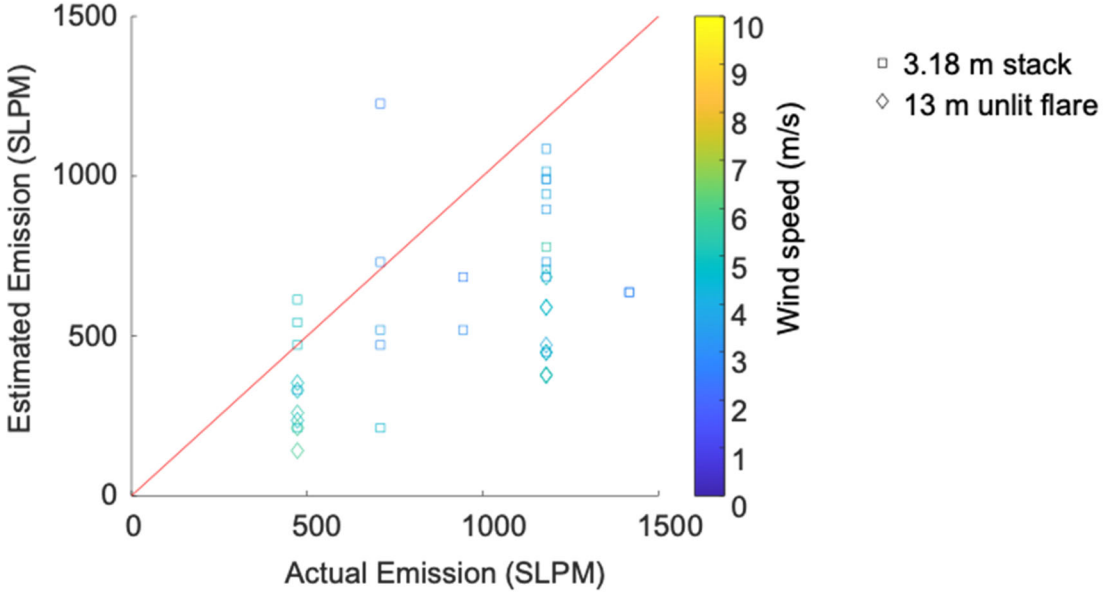

Figure 18: Performance of Airborne SWIR HS (GHGSat).

The wind speed could be inaccurate for two reasons. First, it may be that the modeled wind speed corresponds to a different height than that of the release height. Meteoblue wind speeds are taken at a height of 10 m, while the actual releases occurred at heights of 3 m and 13 m. The provider was not provided the release height, and it is unclear whether the Provider adjusted the Meteoblue wind speed to a presumed emission height (e.g., using a logarithmic scaling function [8]), so, it may be the case that the assumed wind speed is significantly lower than the true wind speed due to release height. Second, the limited accuracy of Meteoblue winds is known to be the leading source of error in other airborne emission measurements [8].

To explore this possibility, Figure 19 shows residual emission of the measurements, with colors corresponding to the difference between the Meteoblue and Kuva wind speeds. There is no apparent trend between the accuracy of the recovered emissions and the residual between the local and Meteoblue wind speeds. Indeed, on April 24, estimates corresponding to larger differences between the Kuva anemometer and the Meteoblue wind speed appear to be more accurate, suggesting that emission accuracy may be due to a different factor. Therefore, the influence of cloud cover appears to be the most likely cause for the systematic underestimation of the emission rate, although further discussion with the service provider/technology developer is needed to confirm this.

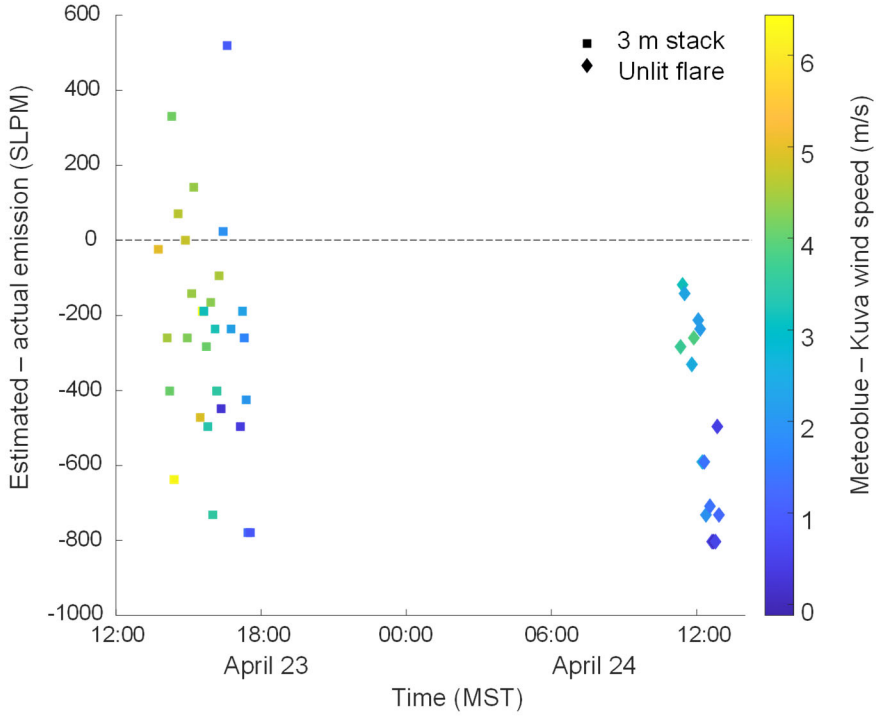

Figure 19: Possible influence of inaccurate wind speed on accuracy of emissions derived from airborne SWIR imaging (GHGSat).

2.4.5 Impact of wind speed on emission accuracy

This section highlights the impact of wind speed on the emission estimates using box plots. Wind speeds are categorized by three wind speed levels, summarized in Table 8, that were derived from even quantiles of all wind speeds recorded over the measurement events. Wind speeds were taken to be those measured using the Kuva ultrasonic anemometer (~16 m above ground), and have not been adjusted for height. Accuracy is represented in terms of the residual emission rate (estimated – actual) as well as the relative emission rate (estimated – actual)/actual. Drone results are excluded due to the low number of measurements carried out using this technology. Note that not all technologies were evaluated over all wind conditions.

Table 8: Wind speed categories

Category	Wind speed range (m/s)
Low	0-2.95
Medium	2.95-5.13
High	5.13-11.52

Box plots are interpreted as follows: the box extends between the first and fourth quartiles of the data (i.e., the box contains 50% of the estimates) while the red line within the box indicates the median value. The ends of the lines indicate the maximum and minimum values of the data, with outliers denoted as symbols.

Figures 20 summarizes performance of AGAT QOGI estimates of releases from the 1.42 m stack and the top of the 2.79 m tank, while Figure 21 shows UW OGI estimates from the 3.18 m stack. Generally, the QOGI technology tends to underestimate the true emission rate, and the error increases with wind speed. As discussed in Section 2.4.2, this trend is attributed principally to the limit imposed by the framerate of the camera.

Figure 22 shows that the Boreal truck measurements (BLS) are highly accurate in low wind conditions, but the variance of estimate error increases significantly with wind speed.

Figure 23 shows the accuracy of emissions from the airborne SWIR hyperspectral imager, which consistently underestimated the ground-truth methane emission rates. This effect is more prominent from the 3.18 m stack versus the 13 m unlit flare stack. As discussed in Section 2.4.4, this may be due to partial cloud cover, although we must consult with the Provider to confirm this hypothesis.

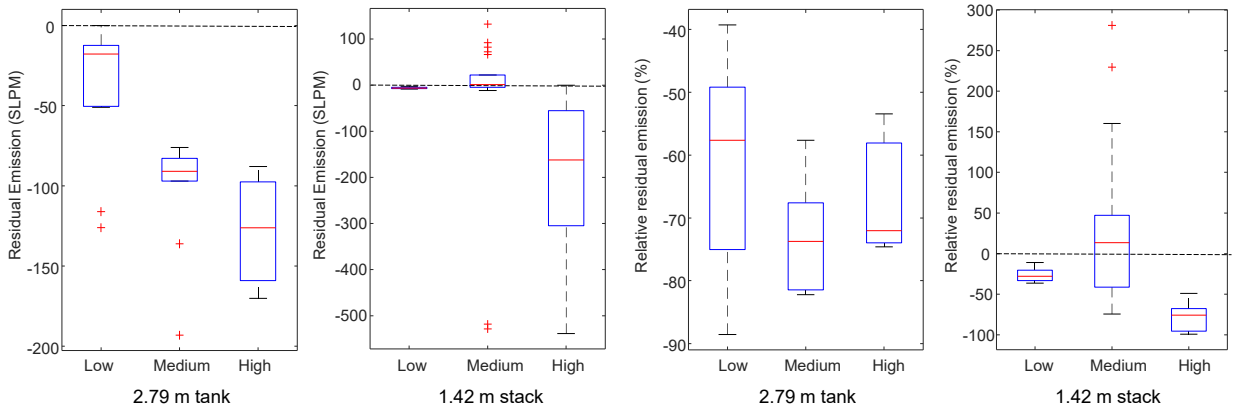

Figure 20: Influence of wind speed on AGAT QOGI emission estimates from the top of the 2.79 m tank and the 1.42 m stack.

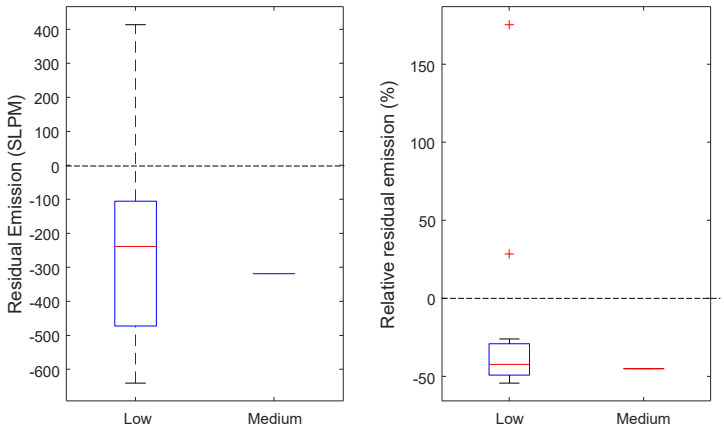

Figure 21: Influence of wind speed on UW QOGI estimates of emissions from the 3.18 m stack.

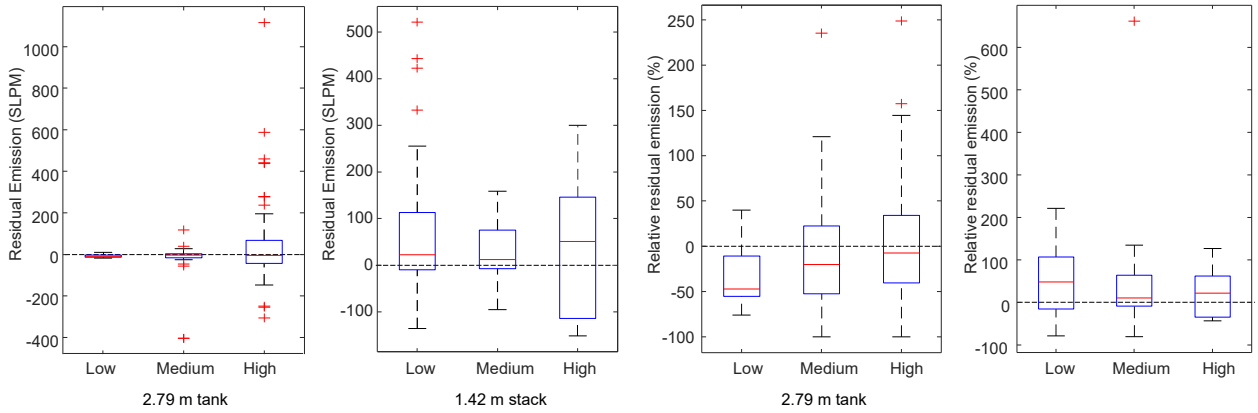

Figure 22: Influence of wind speed on the truck-mounted TDLAS (BLS) emission estimates from the top of the 2.79 m tank and the 1.42 m stack.

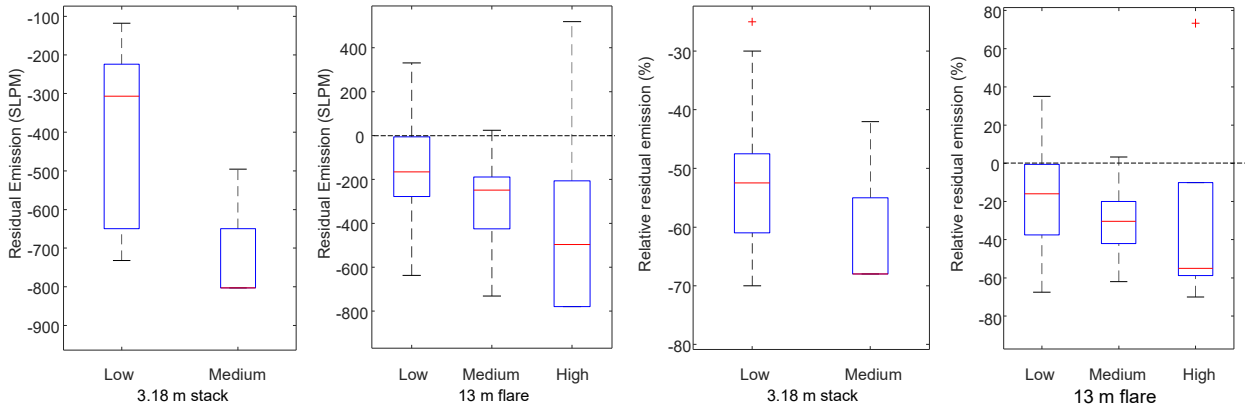

Figure 23: Influence of wind speed on the truck-mounted TDLAS (BLS) emission estimates from the top of the 3.18 m stack and the 13 m unlit flare.

2.4.6: Uncertainty quantification using Bayesian analysis

Data collected from the first field campaign highlights that some experimental parameters (e.g., wind, emission rate, distance) have a considerable influence on the estimated emission rate.

The impact that each parameter, and its associated uncertainty, have on the estimated emission rate can be quantified through Bayesian inference. In this approach the measured data, model parameters, and the quantities-of-interest (methane emission rate, Q_L) are interpreted not as fixed numbers, but random variables that are defined by probability densities.

The first step in this procedure is to define a measurement model. The emission rate indicated by a technology, $Q_{L,d}$, is related to the true emission rate by

$$Q_{L,d} = b\left(Q_L, \boldsymbol{\phi}\right) + \delta b \tag{3}$$

where vector $\boldsymbol{\phi}$ contains n ancillary model parameters (e.g., camera, truck, or drone location), while the error term δb represents both measurement noise as well as model error arising from the incomparability of the presumed model and the true physics. While emission models vary by technology class, they have a general form

$$b = b\left[\mathbf{c}\left(\boldsymbol{\phi}, Q_L\right), u\left(\boldsymbol{\phi}\right)\right] \tag{4}$$

where $\mathbf{c}$ is a vector of concentration measurements (typically from a spectroscopic model) and u is an advection model, e.g., from wind speed measurements, a Gaussian plume model, or, in the case of QOGI, an optical flow algorithm.

Because the error term δb in Equation (3) is unknowable, it is treated as an unbiased normally distributed random variable having a standard deviation σ_b that depends on the leak rate, i.e. $\delta b \sim \mathcal{N}(0, \sigma_b)$. The width of this distribution reflects both the "precision" and "accuracy" of the measurement, since a bias arising from a systematic model error is considered unknowable and thus enveloped into the distribution.

Consequently, the detected emission rate is also normally distributed according to

$$p\left(Q_{L,d} \middle| Q_L, \boldsymbol{\phi}\right) \propto \exp\left\{-\frac{\left[Q_{L,d} - b\left(Q_L, \boldsymbol{\phi}\right)\right]^2}{2\left[\sigma_b\left(Q_L\right)\right]^2}\right\} \tag{5}$$

Equation (5) is the likelihood function, which describes the probability density function (pdf) of observing a measured emission rate $Q_{L,d}$ given the true emission rate Q_L and a set of ancillary parameters $\boldsymbol{\phi}$. The probability density has units inverse to those of Q_L (e.g., hr/kg).

In the absence of prior information about the emission rate, and assuming that the ancillary parameters are perfectly known, we can show that

$$p\left(Q_L \middle| Q_{L,d}, \boldsymbol{\phi}\right) = p\left(Q_{L,d} \middle| Q_L, \boldsymbol{\phi}\right) \tag{6}$$

where $p(Q_L|Q_{L,d}, \boldsymbol{\phi})$ is the *posterior* pdf. The posterior pdf defines what is known about the QOI *after* the measurement. It indicates the certainty of the measured emission rate, provided that: (1) the ancillary model parameters are perfectly known; and (2) nothing else is known about the emission rate beforehand.

However, the ancillary model parameters (e.g., wind speed) are imperfectly known. Accordingly, the parameters in $\boldsymbol{\phi}$ are treated as additional "nuisance" parameters to be inferred along with the emission rate. Obviously, adding these unknowns to the list of inferred variables "diffuses" the pdf and increases the uncertainty in the inferred Q_L estimate, so it is important to incorporate any information about both $\boldsymbol{\phi}$ and Q_L that is available before the measurement into the inference procedure. This information is encoded as a prior probability density for each variable, and, assuming that these parameters are mutually independent, an overall prior pdf is given by

$$p_{pr}\left(Q_L, \boldsymbol{\phi}\right) = p_{pr}\left(Q_L\right) \cdot \prod_{j=1}^{n} p_{pr}\left(\phi_j\right) \tag{7}$$

The likelihood, prior, and posterior pdfs are related by Bayes' equation

$$p\left(Q_L, \boldsymbol{\phi} \middle| Q_{L,d}\right) = \frac{p\left(Q_{L,d} \middle| Q_L, \boldsymbol{\phi}\right) p_{pr}\left(Q_L, \boldsymbol{\phi}\right)}{p\left(Q_{L,d}\right)} \tag{8}$$

where the evidence

$$p\left(Q_{L,d}\right) = \int_{Q_L, \boldsymbol{\phi}} p\left(Q_{L,d} \middle| Q_L, \boldsymbol{\phi}\right) p_{pr}\left(Q_L, \boldsymbol{\phi}\right) \mathrm{d}Q_L \mathrm{d}\boldsymbol{\phi} \tag{9}$$

ensures that the posterior pdf satisfies the Law of Total Probability.

The outcome of Equation (8) is an n+1 dimension joint pdf that defines what is known about both Q_L and $\boldsymbol{\phi}$ after the measurements. In practice, however, we are interested only in a pdf for Q_L, which can be found through marginalizing over the nuisance parameters

$$p\left(Q_L \middle| Q_{L,d}\right) = \int_{\boldsymbol{\phi}} p\left(Q_L, \boldsymbol{\phi} \middle| Q_{L,d}\right) d\boldsymbol{\phi} \tag{10}$$

It may be further simplified by defining a credible interval that may be interpreted as containing the "true" emission rate with a specified probability, e.g., 90%, as shown in Figure 24.

The Bayesian approach presents several key benefits for quantifying methane emissions:

1. It provides a comprehensive definition of what is known about an emission rate given an indicated emission rate and uncertain model parameters. This information is particularly important when allocating resources to reduce emissions, or in a regulatory context.
2. The width of the credible intervals is a ready measure of the accuracy/reliability of a measurement technique, which may then be used to compare the performance of technologies and design cost-effective FEMPs.
3. It explicates the role of prior information and other assumptions in deriving the flux estimates. This prior information may be revised as more information becomes available.

While the above framework may be applied to any technology, preliminary work has focused on truck mounted TDLAS measurements using the IGM because: (1) the IGM measurement model is the simplest of the approaches evaluated to date: (2) the Technology Provider has provided the raw data needed to define appropriate priors and the likelihood function.

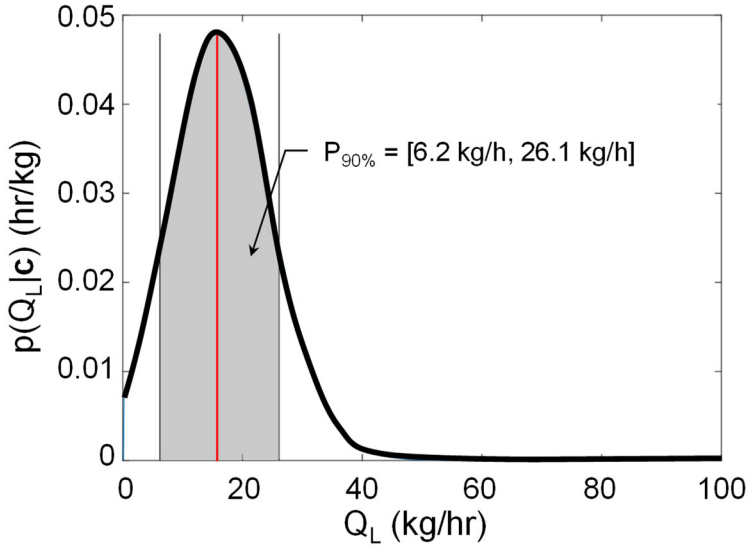

Figure 24: Posterior probability density function of the estimated emission rate Q_L knowing a set of concentration measurements, **c**. The maximum a posteriori (MAP) estimate for the emission rate is 18 kg/hr (red vertical line) and the credible interval (black vertical lines) is [6.2 kg/hr – 26.1 kg/hr] so that the estimated emission rate has 90% probability of being contained in that interval. This plot was generated based on a numerical simulation of a stack natural gas emission of 20 kg/hr and a virtual truck-based measurement. The IGM method was used to infer Q_L and only the wind speed was considered as an uncertain parameter with uncertainty of 0.5 m/s.

Preliminary results were presented at the Joint Congress of the Canadian Meteorological and Oceanographic Society (CMOS), Canadian Geophysical Union (CGU), and the Eastern Snow Conference (ESC), held on June 1-3, 2022 [20]. This analysis relied on synthetic concentration measurements and wind speeds derived from a CFD large eddy simulation of a methane plume.

Ongoing work is focused on developing the required prior pdfs and measurement model needed to interpret the truck mounted TDLAS data, through a combination of theoretical analysis and empirical studies. Finally, the emission rates reported in Sec. 2.4.3 (Table 6) will be compared with the marginalized posterior pdf, Eq. (10), to confirm the veracity of the Bayesian analysis. (E.g., one expects that 90% of the measurements to lie within the 90% credibility interval.) If time permits, this approach will be extended to other measurement technologies.

3. PRELIMINARY CONCLUSIONS

To date, research activities have focused on: developing a comprehensive list of methane emission quantification technologies (phase 1); evaluating these technologies through laboratory-based measurements (phase 2); design and execution of the first field campaign (phase 3); design of the second field campaign (phase 3); a preliminary statistical analysis of the data from the first field campaign (phase 4); and establishing a Bayesian framework for uncertainty quantification (phase 4).

Results from the first field campaign highlight the different capabilities of the measurement techniques and their susceptibility to various environmental factors. For example, QOGI technologies are best suited to measure smaller releases, while the airborne SWIR imaging works well for larger releases. The truck mounted TDLAS system performed well for all release rates.

The truck mounted TDLAS system provided the most unbiased estimates and appeared least susceptible to environmental factors. The accuracy of QOGI estimates degraded at higher wind speeds and flow rates, likely due to the limited framerate of the camera. The OGI estimates were also significantly less accurate for tank releases, possibly because of the large distance between the release and the camera/operator. The airborne SWIR system systematically underestimated emission rates. Although the exact cause of this bias is unclear, it may be related to suboptimal sky conditions during the measurements.

When interpreting these results, it is important to understand the context of the measurements and how they may depart from real-world conditions. For example, the truck operator knew both the location and height of the releases and was therefore able to adjust their plume transits accordingly, while, during an actual survey, they may only have a general understanding of the location of a candidate emission source, or there may be more than one source. Moreover, the truck will be confined to nearby roads, which may not be oriented in a manner conducive to a plume measurement. Likewise, the drone operator would likely spend more time than the ~20 minutes allotted during the field measurements to characterize a single plume, and, under real-world conditions, the aircraft operator may wait for clearer skies to carry out their measurements.

Crucially, the objective of the field campaign is *not* to conclude that one technology is "better" than the other. Instead, field measurements serve to evaluate performance of candidate technologies under industrially relevant yet well-defined conditions on an individual basis, and to assess their sensitivity to uncertain environmental factors. These results will be compared with statistical models that provide both an emission estimate as well as associated uncertainties. Understanding the uncertainties associated with emission quantification technologies is critical when making decisions about the cost effectiveness of candidate fugitive emission management plans (FEMPs), when compiling an emissions inventory, and when assessing regulatory compliance.

In terms of statistical modeling, work has focused on developing a Bayesian framework for estimating methane emissions using truck mounted TDLAS measurements and an inverse Gaussian plume model. Preliminary results have been derived from synthetic concentration measurements developed from a CFD-large eddy simulation of a methane plume. Ongoing work is focused on assessing the experimentally derived TDLAS measurements with the Bayesian model, and extending this approach to other measurement systems.

4. FUTURE WORK

Future work is focused on three principal areas: (1) the second field campaign; (2) statistical data analysis; and (3) alternative FEMP equivalency modelling.

4.1 Second field campaign

The second field campaign is tentatively planned for September 25-October 1, with fallback dates of October 17-23. The team is planning to include three aircraft-conveyed technologies, a truck-based provider, as well as additional QOGI team. Several of the technology providers who participated in the first field campaign have been invited to participate in the second field campaign. The second campaign will be designed to assess the consistency in the performance of the technologies from the first field campaign, and to fill in gaps in wind speed and emission rates.

4.2 Statistical data analysis

The preliminary statistical analysis presented in Section 2.4 will be augmented with the results of the second field campaign. For each emission quantification technology, measured emission rates will be modelled against the true release rates using various statistical models. The variables which were found to impact the precision and accuracy of measured emission rates in this report, such as the wind speed, will be included in the models. Different models such as generalised linear models and hierarchical Bayesian models will be explored and the model which most accurately models the errors will be chosen to give final estimates of uncertainty.

4.2 Alternative FEMP equivalency modeling

The alternative FEMP equivalency modelling will test the potential for application of various emission quantification technologies in a FEMP. Both a default FEMP (as per Alberta Energy Regulator Directive 060) and various alternative FEMPs will be modelled and feasibility of a technology's use in an alternative FEMP will be determined by comparison of the quantity of fugitive emissions to those released in the default FEMP. Modelling will be completed using Arolytics's proprietary AroFEMP simulation tool and the data from the Fugitive Emission Management Program Effectiveness Assessment Study.

REFERENCES

[1] D. Risk, K. MacKay, M. Laboie and E. Bourlon, "Methane Emissions Data Aggregation and Analysis Project for FEMP-EA and Canadian context: Resources, patterns, and measurement methodology performance," PTAC, Calgary, Alberta, 2019.

[2] B. Horn and B. G. Schunck, "Determining Optical Flow," *Artificial Intelligence,* vol. 17, p. 185–203, 1981.

[3] B. D. Lucas and T. Kanade, "An iterative image registration technique with an application to stereo vision," in *International Joint Conference on Artificial Intelligence*, Vancouver BC, 1981.

[4] G. Durant, P.-Y. Foucher, S. Doz, X. Watremez, S. Jourdan, E. Vanneau and H. Pinot, "Test of SIMAGAZ: a LWIR cryogenic multispectral infrared camera for methane gas leak detection and quantification SPIE 11727, Algorithms, Technologies, and Applications for Multispectral and Hyperspectral Imaging XXVII," in *Proceedings Volume 11727, Algorithms, Technologies, and Applications for Multispectral and Hyperspectral Imaging XXVII*, 2021.

[5] B. Kura and A. Jilla, "Feasibility of the Inverse-Dispersion Model for Quantifying Drydock Emissions," *Atmosphere,* vol. 10, p. 328, 2019.

[6] D. R. Caulton, Q. Li, E. Bou-Zeid, J. P. Fitts, L. M. Golston, D. Pan, J. Lu, H. M. Lane, B. Buchholz, X. Guo, J. McSpiritt, L. Wendt and M. A. Zondlo, "Quantifying uncertainties from mobile-laboratory-derived emissions of well pads using inverse Gaussian methods," *Atmos. Chem. Phys.,* vol. 18, pp. 15145-15168, 2018.

[7] United States Environmental Protection Agency, "Standards of Performance for New, Reconstructed, and Modified Sources and Emissions Guidelines for Existing Sources: Oil and Gas Sector Climate Review," *Fed. Reg.,* vol. 86, p. 63310, 2021.

[8] M. R. Johnson, D. R. Tyner, S. Conley, S. Schwietzke and Zavala-Araiza, "Comparisons of Airborne Measurements and Inventory Estimates of Methane Emissions in the Alberta Upstream Oil and Gas Sector," *Environ. Sci. Technol.,* vol. 51, pp. 13008-13017, 2017.

[9] D. J. Varon, D. J. Jacob, J. McKeever, B. O. A. Durak, Y. Xia and Y. Huang, "Quantifying methane point sources from fine-scale satellite observations of atmospheric methane plumes," *Atmos. Meas. Tech.,* vol. 11, pp. 5673-5686, 2018.

[10] O. A. Sherwood, S. Schwietzke, V. A. Arling and G. Etiope, "Global inventory of gas geochemistry data from fossil fuel, microbial and burning sources, version 2017," *Earth Syst. Sci. Data,* vol. 9, pp. 639-656, 2017.

[11] M. Nightengale, Interviewee, *Personal communication.* [Interview]. 08 03 2022.

[12] J. D. Wilson and B. L. Sawford, "Review of Lagrangian stochastic models for trajectories in the turbulent atmosphere," *Boundary-Layer Meterol.,* vol. 78, pp. 191-210, 1996.

[13] B. Crenna, "An Introduction to WindTrax," Department of Earth and Atmospheric Science, the University of Alberta, Calgary, 2006.

[14] Bonifacio et al., "Comparison of AERMOD and WindTrax dispersion models in determining PM10 emission rates from a beef cattle feedlot," *Journal of Air and Waste Management Association,* vol. 63, no. 5, 2013.

[15] Hrad et al., "Comparison of forward and backward Lagrangian transport modelling to determine methane emissions from anaerobic digestion facilities," *Atmospheric Environment: X,* vol. 12, 2021.

[16] T. K. Flecsh, J. D. Wilson and E. Yee, "Backward-Time Lagrangian Stochastic Dispersion Models and Their Application to Estimate Gaseous Emissions," *Journal of Applied Meteorology and Climatology,* vol. 34, no. 6, pp. 1320-1332, 1995.

[17] A. P. Ravikumar, J. Wang, M. McGuire, C. S. Bell, D. Zimmerle and A. R. Brandt, "'Good versus Good Enough?' Empirical Tests of Methane Leak Detection Sensitivity of a Commercial Infrared Camera," *Environ. Sci. Technol.,* vol. 52, pp. 2368-2374, 2018.

[18] S. Schwietzke, M. Harrison, T. Lauderdale, K. Branson, S. Conley, F. C. George, D. Jordan, G. R. Jersey, C. Zhang, H. L. Mairs, G. Pétron and R. C. Schnell, "Aerially Guided Leak Detection and Repair: A Pilot Field Study for Evaluating the Potential of Methane Emission Detection and Cost-Effectiveness," *J. Air Waste Manag. Assoc.,* vol. 69, pp. 71-88, 2019.

[19] D. R. Tyner and M. R. Johnson, "Where the Methane Is-Indisghts from Novel Airborne LiDAR Measurements Combined with Ground Survey Data," *Environ. Sci. Technol.,* vol. 55, pp. 9773-9783, 2021.

[20] P. Lapeyre, D. Blackmore, M. Nagorski and K. J. Daun, "A statistical framework for uncertainty estimation when quantifying methane emissions (presentation)," in *Joint Congress of the Canadian Meteorological and Oceanographic Society (CMOS), Canadian Geophysical Union (CGU), and the Eastern Snow Conference (ESC)*, Virtual, 2022 .